Macroscopic Visualization of the Heart Electrical Activity Via an Algebraic Computer Model

A. Ghaffari*, M. R. Homaeinezhad**, Y. Ahmadi**, M. Rahnavard** and R. Rahmani***

Abstract: In this study, a mathematical model is developed based on algebraic equations which is capable of generating artificially normal events of electrocardiogram (ECG) signals such as P-wave, QRS complex, and T-wave. This model can also be implemented for the simulation of abnormal phenomena of electrocardiographic signals such as ST-segment episodes (i.e. depression, elevation, and sloped ascending or descending) and repolarization abnormalities such as T-Wave Alternans (TWA). Event parameters such as amplitude, duration, and incidence time in the conventional ECG leads can be a good reflective of heart electrical activity in specific directions. The presented model can also be used for the simulation of ECG signals on torso plane or limb leads. To meet this end, the amplitude of events in each of the 15-lead ECG waveforms of 80 normal subjects at MIT-BIH Database (www.physionet.org) are derived and recorded. Various statistical analyses such as amplitude mean value, variance and confidence intervals calculations, Anderson-Darling normality test, and Bayesian estimation of events amplitude are then conducted. Heart Rate Variability (HRV) model has also been incorporated to this model with HF/LF and VLF/LF waves power ratios. Eventually, in order to demonstrate the suitable flexibility of the presented model in simulation of ECG signals, fascicular ventricular tachycardia (left septal ventricular tachycardia), rate dependent conduction block (Aberration), and acute Q-wave infarctions of inferior and anterior-lateral walls are finally simulated. The open-source simulation code of above abnormalities will be freely available.

Keywords: Electrocardiogram(ECG), Mathematical Model, Heart Arrhythmia, Simulation.

1 Introduction

First models of heart refer to middle age and renaissance era depicted in the Leonardo da Vinci's drawings [1]. Generally, modeling is an abstraction by which it would be possible to move from the known to the unknown as to the resulted model is consistent with observations and can be used for the prediction of unobserved set. The major aims of modeling can be summarily stated as management and control, prediction and simulation of phenomena, as well as education and familiarity with complicated understudy phenomena [1,

2]. Modeling of the electrical activity of heart as a complicated system can be conducted using microscopic methods which are based on cellular structure and dynamics, cellular automata [3], and reaction diffusion systems [4], or macroscopic approaches which are based on observed electrical behavior of the heart on the skin surface [5, 6]. Single-lead [5], multi-lead [7] and high-resolution multi-lead [8, 9] electrocardiographic signals as electrical skin surface recordings can be a useful way in the macroscopic modeling of the heart. Some events in the electrocardiogram signals are indicators of specific electrocardiographic occurrences, the most typical of which in normal conditions are P-wave, QRS complex, and T-wave (Sometimes U-wave) that happen relative to each other with regular duration. Furthermore, the morphology of P, QRS, and T waves can vary in different leads regarding the fact that each lead illustrates a distinct picture of the heart electrical activity in a specific direction [10, 11]. For instance, when the ventricular septum is normally depolarized from the left side to the right side, R-wave and Q-wave will be observed in chest leads V_1 and V_6, respectively.

However, in the depolarization of the ventricular main muscle mass, S-wave and R-wave will instead be seen in leads V_1 and V_6 [10]. Depending upon the distance and orientation of the lead relative to the heart, the amplitudes of waves in each lead will differ from those in the other leads [10, 12].

The aim of this study is to achieve knowledge about the distribution of wave amplitudes relative to each other in a single ECG lead and relative to their corresponding waves in the other leads as well as developing a model based on this information in order to simulate some normal and abnormal events. To meet this end, the amplitude of events in each of the 15-lead ECG waveforms of 80 normal subjects at MIT-BIH Database (**www.physionet.org**) are derived and recorded. Various statistical analyses such as amplitude mean value, variance and the corresponding confidence intervals calculations, Anderson-Darling normality test [13], and Bayesian estimation of events amplitude are then conducted. A Gaussian (normal) probability density function (pdf) is then assumed for each of event differences with mean values and variances obtained from statistical analyses. Afterwards, a Bayesian estimator of the elevation of each event in all leads is designed with the amplitude of P-wave in lead 1 as an input. If so, the 15-lead ECG signal generator will consequently be created. In order to simulate the interaction of regulating sympathetic and parasympathetic mechanisms in the modulation of QRS complexes, the original work of McSharry-Clifford (2003) [5] is used in the next step and waves with HF/LF and VLF/LF power ratios (HF: high frequency, LF: low frequency and VLF: very low frequency), are incorporated to the power spectrum of RR-tachogram [5, 14]. The resulted algebraic model of this study has the following characteristics:

- The model parameters have independent effects on the model output events, i.e. the amplitude, duration, and incidence time of each event can directly be considered as inputs to the program.

- This model is capable of generating transient ST-segment episodes such as depression, elevation, and sloped ascending or descending, [15].

- This model consists of algebraic mathematical equations Therefore, there would be no need to numerical solution routines.

Finally, to illustrate the capabilities and flexibility of the presented model in generating artificial arrhythmias and ECG signal abnormalities, fascicular ventricular tachycardia (left septal ventricular tachycardia), rate dependent conduction block (Aberration), and acute Q-wave infarctions of inferior and anterior-lateral walls

are simulated. The open source simulation code of the aforementioned abnormalities will be freely available.

2   Statistical Analysis of Wave Amplitudes

For the aim of statistical analyses of events amplitudes and finding the corresponding relation between them in each lead, the 15-lead ECG data of 80 normal subjects were derived from the MIT-BIH DATABASE (www.physionet.org). The position of electrodes on the body surface related to each lead can be seen in Fig. 1. The wave amplitudes of each lead were then obtained and recorded by implementing the wave detection algorithm of WaveForm DataBase (WFDB), [16]. The difference between the events amplitudes, i.e. P-Q, P-R, P-S, P-T, Q-R, Q-S, Q-T, R-S, R-T, and S-T were then calculated for all 15-lead ECGs. It should be noted that Q-waves were not observed in some leads such as MLV1, MLV2, and MLV3 (see Table 2). Statistical analyses such as mean value and variance, and the corresponding confidence intervals calculations were then conducted as follows.

Confidence interval (CI) of a parameter which has wide applications in engineering statistical analyses is actually an interval estimate of that parameter and has two characteristics: First, the point estimation of the parameter is located in this interval. Second, there would be a high probability for the true value of the parameter to belong to this interval. In this study, the results of the CI and variance calculations will be presented. More information about the CI and variance equations and the corresponding calculations can be found at [13].

To calculate the CI, it can be shown that if $\hat{\mu}_{SM}$ and $\hat{\sigma}_{SV}^2$ represent the mean value and variance of n number of samples from a random population ($\mathbf{X} = x_1, x_2, ..., x_n$) with normal distribution and unknown variance, then a confidence interval of $100(1-\alpha)$ % for the true mean value of observations, μ_T, can be obtained from the following equations, [13],

$$\hat{\mu}_{SM} - \frac{t(\alpha/2, n-1)\,\hat{\sigma}_{SV}}{\sqrt{n}} \leq \mu_T \tag{1}$$

$$\mu_T \leq \hat{\mu}_{SM} + \frac{t(\alpha/2, n-1)\,\hat{\sigma}_{SV}}{\sqrt{n}}$$

where

$$\begin{cases} \hat{\mu}_{SM} = \dfrac{1}{n}\sum_{k=1}^{n} x_i \\ \hat{\sigma}_{SV}^2 = \dfrac{1}{n-1}\sum_{k=1}^{n}\left(x_i - \hat{\mu}_{SM}\right)^2 \end{cases} \tag{2}$$

in which, $t(\tau, n)$ is $100 \times \tau$ percentage point from t-distribution of n degrees of freedom and can be obtained from the following equation

$$\int_{t(\alpha,n)}^{+\infty} p_T(t,n)\,dt = \alpha \qquad (3)$$

and,

$$p_T(t,n) = \frac{\Gamma\left[(n+1)/2\right]}{\sqrt{\pi n}\,\Gamma(n/2)} \frac{1}{\left[(t^2/n)+1\right]^{(k+1)/2}} \qquad (4)$$

$$-\infty < t < +\infty$$

Also to find the CI for the variance, If $\hat{\mu}_{SM}$ and $\hat{\sigma}_{SV}^2$ represent the mean value and variance of n number of samples from a random population with normal distribution ($\mathbf{X} = x_1, x_2, ..., x_n$) and with unknown variance, then a confidence interval of 100(1-α) % for the true variance of observations, σ_T^2, can be obtained from the following equation

$$\frac{(n-1)\hat{\sigma}_{SV}^2}{\chi^2(\alpha/2, n-1)} \le \hat{\sigma}_T^2 \le \frac{(n-1)\hat{\sigma}_{SV}^2}{\chi^2(1-\alpha/2, n-1)} \qquad (5)$$

where $\chi^2(\alpha/2, n-1)$ and $\chi^2(1-\alpha/2, n-1)$ are the upper and lower 100×α/2 percentile points of the chi-square distribution of degrees of freedom n-1, respectively, and can be calculated as, [13]

$$\int_{\chi^2(\alpha,n)}^{+\infty} p_{\chi^2}(x,n)\,dx = \alpha \qquad (6)$$

$$p_{\chi^2}(x,n) = \frac{1}{2^{n/2}\Gamma(n/2)} x^{(n/2)-1} e^{-x/2}, \quad x > 0 \qquad (7)$$

2.1 Anderson- Darling Distance Test

In many applications, in order to provide the required prerequisites for the design of estimation and identification algorithms, we need to determine a distribution function which most probably describes the distribution of conducted observations. On the other hand, if the probability density function is considered for the observations set $\mathbf{\Omega}$, the structure of the corresponding estimator will implicitly be determined. In this study, a method called Anderson-Darling Distance Test (ADDT) is used for the calculation of goodness of fit relative to normal distribution. In this method, a statistic is defined on the basis of the following integral transform

$$F(x) = \int_{-\infty}^{x} p(s)\,ds \qquad (8)$$

Using the mapping in the above integral, a certain distribution with the density $p(x)$ is converted to a uniform distribution. If so, it can be concluded that for independent and identically distributed (i.i.d.) random variables x_1, x_2,…, x_n with cumulative distribution function (CDF) of F(x), the functions F(x_1), F(x_2),…, F(x_n) will be independent uniform random variables in the interval (0,1). In fact, Anderson-Darling Distance Test indicates how much closer is the value of F(x_1), F(x_2),…, F(x_n) to the uniform distribution in the interval (0,1) [13].

In the ADDT it is assumed that the observation domain data are the members of a discrete random variable. For each $x \in \mathbf{\Omega}$, the value of $F(\mathbf{X} \le x)$ is then calculated and restored. The best straight line crossing the points (x, F(x)) was next determined. The mean absolute distance value of the points relative to this line can be obtained as

$$AD_{MAD}^{(R)} = \frac{1}{n}\sum_{i=1}^{n}\left|F(x_i) - L(x_i)\right| \qquad (9)$$

where $L(x)$ represents the equation of the line in the (x, F(x)) plane. Using the Monte-Carlo algorithms [17], a sequence of the numbers belonging to a normal random population with known mean value and variance of the observation set was generated. The parameter $AD_{MAD}^{(N)}$ for this sequence will then be calculated from the line $L(x)$. Afterwards, the fraction $AD_{MAD}^{R}/AD_{MAD}^{N}$ is determined and compared with a specific threshold. If the fraction is greater than τ, the normality assumption will be rejected. In this study, the value $\tau = 2.2$ is selected and the results of the normality test for the differences T-P, R-Q, and R-P are presented in Tables 1 to 3. In Figs. 2 and 3, the probability $F(\mathbf{X} \le x)$ versus observation domains is plotted for the leads II and V_x. According to ADDT, when the values of probability $F(\mathbf{X} \le x)$ are remarkably far from the straight line $L(x)$ or build a curvature, the normality assumption for the data distribution cannot be acceptable. This can be observed in the Figs. 2 and 3.
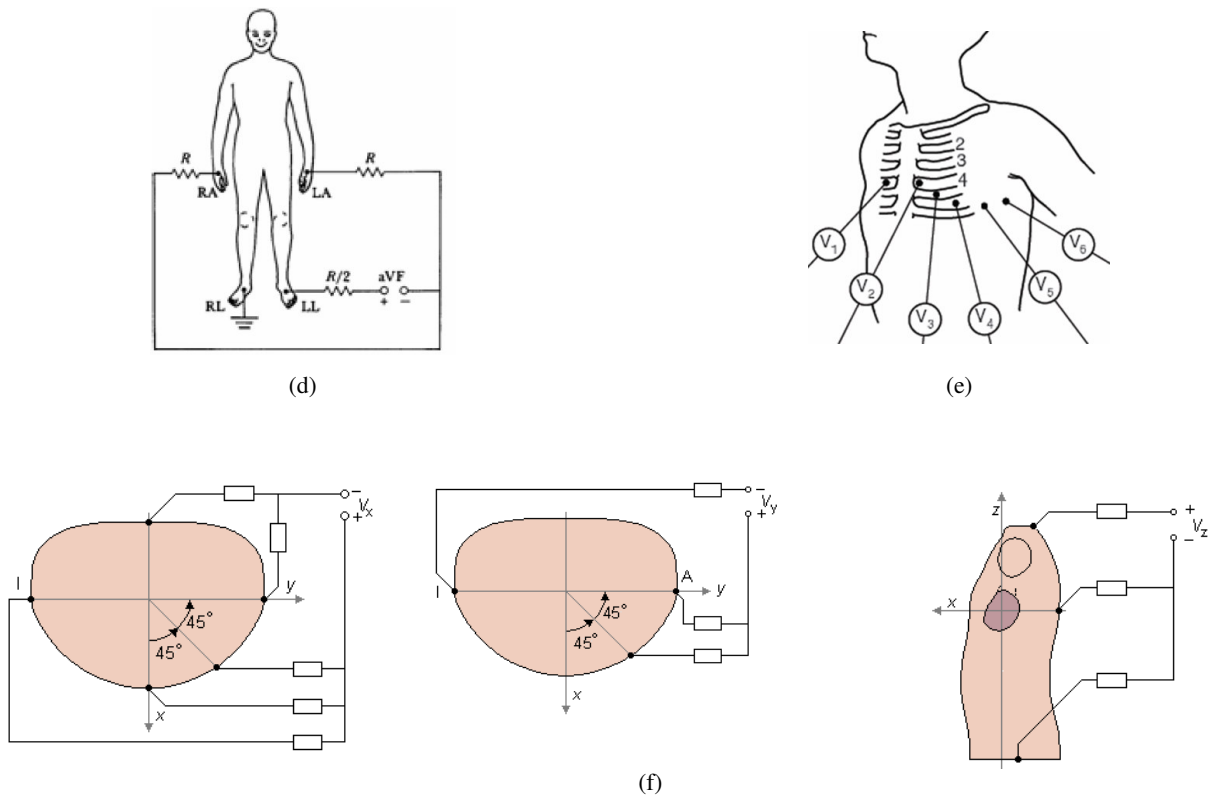

(a)   (b)   (c)
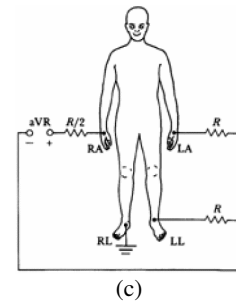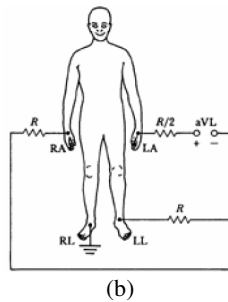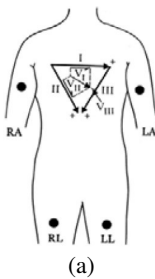
Fig. 1. Overview of the landmarks used for the generation of heart electrical pictures; (a) Limb Leads I, II and III, (b) Lead avL, (c) Lead avR, (d) Lead avR [18], (e) Chest Leads [10], (f) Frank V_x, V_y and V_z leads [19]

Table 1. Results of the statistical analyses conducted on the T-wave and P-wave amplitudes differences for the 15-lead ECGs: Mean value, variances, the corresponding confidence intervals with the value of $\alpha = 0.05$ and Anderson-Darling Normality Test using a threshold $\tau = 2.2$.

Data	1st and 2nd Order Moments		Confidence Intervals ($\alpha = 0.05$)		Normality Test (Anderson-Darling Distance Test)			
	Mean (μ)	Variance(σ^2)	Mean CI 100 (1-α)%	Variance CI 100 (1-α)%	Real Data (A)	Ideal Normal (B)	Ratio A/B	Test Result
(MLI)	0.1763	0.0079	(0.1534,0.1938)	(0.0059,0.0112)	0.2340	0.1587	1.4744	Accepted
(MLII)	0.2080	0.0179	(0.1776,0.2383)	(0.0133,0.0252)	0.1248	0.1229	1.0155	Accepted
(MLIII)	0.0547	0.0095	(0.0281,0.0812)	(0.0067,0.0144)	1.1155	0.5180	2.1533	Accepted
(MLAVR)	-0.1942	0.0082	(-0.2148,-0.1736)	(0.0061,0.0116)	0.2447	0.1175	2.0832	Accepted
(MLAVL)	0.0823	0.0034	(0.0667,0.0978)	(0.0024,0.0051)	0.7089	0.2773	2.5566	Rejected
(MLAVF)	0.1120	0.0124	(0.0865,0.1375)	(0.0092,0.0176)	0.3340	0.1871	1.7851	Accepted
(MLV1)	-0.0534	0.0097	(-0.0820,-0.0248)	(0.0067,0.0153)	0.4477	0.1331	3.3639	Rejected
(MLV2)	0.4544	0.0594	(0.3979,0.5108)	(0.0440,0.0846)	0.1271	0.1587	0.8007	Accepted
(MLV3)	0.5938	0.0691	(0.5342,0.6535)	(0.0515,0.0977)	0.0979	0.1154	0.8486	Accepted
(MLV4)	0.6068	0.0603	(0.5503,0.6633)	(0.0447,0.0856)	0.1164	0.1050	1.1080	Accepted
(MLV5)	0.4701	0.0457	(0.4216,0.5186)	(0.0341,0.0646)	0.1296	0.1237	1.0476	Accepted
(MLV6)	0.3029	0.0301	(0.2640,0.3418)	(0.0225,0.0424)	0.1530	0.1083	1.4137	Accepted
(MLVX)	0.3370	0.0277	(0.2992,0.3748)	(0.0207,0.0392)	0.1308	0.1232	1.0167	Accepted
(MLVY)	0.1343	0.0111	(0.1101,0.1585)	(0.0082,0.0157)	0.1515	0.0849	1.7859	Accepted
(MLVZ)	-0.2139	0.0146	(-0.2421,-0.1857)	(0.0108,0.0209)	0.1067	0.0782	1.3642	Accepted

Table 2. Results of the statistical analyses conducted on the R-wave and Q-wave amplitudes differences for the 15-lead ECGs: Mean value, variances, the corresponding confidence intervals with the value of $\alpha = 0.05$ and Anderson-Darling Normality Test using a threshold $\tau = 2.2$.

Data	1st and 2nd Order Moments		Confidence Intervals (α = 0.05)		Normality Test (Anderson-Darling Distance Test)			
	Mean (μ)	Variance(σ²)	Mean CI 100 (1-α)%	Variance CI 100 (1-α)%	Real Data (A)	Ideal Normal (B)	Ratio A/B	Test Result
(MLI)	0.7130	0.0822	(0.6395,0.7864)	(0.0592,0.1219)	0.1733	0.1100	1.5744	Accepted
(MLII)	1.2236	0.2502	(1.0986,1.3485)	(0.1815,0.3669)	0.4335	0.2339	1.8534	Rejected
(MLIII)	1.0136	0.3233	(0.8520,1.1752)	(0.2256,0.5021)	0.1982	0.1310	1.5128	Accepted
(MLAVR)	0.8814	0.0621	(0.8192,0.9437)	(0.0451,0.0911)	0.5202	0.1888	2.7551	Rejected
(MLAVL)	0.4921	0.0623	(0.4088,0.5753)	(0.0412,0.1052)	0.3542	0.1220	2.9029	Rejected
(MLAVF)	1.0058	0.3392	(0.8540,1.1576)	(0.2431,0.5065)	0.1614	0.0894	1.8051	Accepted
(MLV1)	No Q-Wave				--	--	--	--
(MLV2)	No Q-Wave				--	--	--	--
(MLV3)	No Q-Wave				--	--	--	--
(MLV4)	1.7188	0.5441	(1.3396,2.0981)	(0.3018,1.2603)	0.1913	0.0996	1.9202	Accepted
(MLV5)	1.8301	0.5462	(1.6340,2.0262)	(0.3893,0.8220)		0.1936	1.5668	Accepted
(MLV6)	1.3289	0.4722	(1.1626,1.4952)	(0.3457,0.6838)	0.2547	0.1310	1.9440	Accepted
(MLVX)	1.3255	0.3053	(1.1875,1.4636)	(0.2215,0.4479)	0.3615	0.1871	1.9321	Accepted
(MLVY)	1.0319	0.2316	(0.9030,1.1608)	(0.1646,0.3500)	0.2224	0.1499	1.4863	Accepted
(MLVZ)	1.0809	0.1043	(1.0086,1.1533)	(0.0780,0.1466)	0.0894	0.0804	1.1119	Accepted

Table 3. Results of the statistical analyses conducted on the R-wave and P-wave amplitudes differences for the 15-lead ECGs: Mean value, variances, the corresponding confidence intervals with the value of $\alpha = 0.05$ and Anderson-Darling Normality Test using a threshold $\tau = 2.2$.

| Data	1st and 2nd Order Moments		Confidence Intervals (α = 0.05)		Normality Test (Anderson-Darling Distance Test)			
	Mean (μ)	Variance(σ²)	Mean CI 100 (1-α)%	Variance CI 100 (1-α)%	Real Data (A)	Ideal Normal (B)	Ratio A/B	Test Result
(MLI)	0.5140	0.0580	(0.4593,0.5687)	(0.0432,0.0820)	0.1394	0.1154	1.2080	Accepted
(MLII)	0.9045	0.2137	(0.7996,1.0094)	(0.1592,0.3019)	0.2292	0.1294	1.7713	Accepted
(MLIII)	0.6635	0.2702	(0.5315,0.7955)	(0.1951,0.3990)	0.1904	0.0997	1.9106	Accepted
(MLAVR)	0.2248	0.0069	(0.2041,0.2456)	(0.0050,0.0101)	0.6235	0.2568	2.4275	Rejected
(MLAVL)	0.2740	0.0429	(0.2204,0.3275)	(0.0308,0.0638)	0.2656	0.1395	1.9047	Accepted
(MLAVF)	0.7073	0.2520	(0.5926,0.8220)	(0.1874,0.3570)	0.1929	0.1044	1.8741	Accepted
(MLV1)	0.3441	0.0269	(0.3047,0.3835)	(0.0197,0.0388)	0.1648	0.1347	1.2236	Accepted
(MLV2)	0.5342	0.0773	(0.4711,0.5973)	(0.0576,0.1093)	0.1600	0.1100	1.4540	Accepted
(MLV3)	0.7773	0.1522	(0.6888,0.8659)	(0.1134,0.2151)	0.1125	0.0902	1.2479	Accepted
(MLV4)	1.2653	0.3510	(1.1300,1.4007)	(0.2611,0.4973)	0.0760	0.0877	0.8667	Accepted
(MLV5)	1.5217	0.4322	(1.3734,1.6699)	(0.3226,0.6092)	0.3700	0.1256	2.9459	Rejected
(MLV6)	1.1426	0.3775	(1.0050,1.2802)	(0.2823,0.5309)	0.3653	0.1943	1.8802	Accepted
(MLVX)	1.1201	0.2420	(1.0084,1.2317)	(0.1803,0.3420)	0.4230	0.2079	2.0346	Accepted
(MLVY)	0.6835	0.1712	(0.5883,0.7787)	(0.1271,0.2432)	0.1612	0.1009	1.5971	Accepted
(MLVZ)	0.7226	0.0817	(0.6568,0.7883)	(0.0607,0.1161)	0.1543	0.1291	1.1952	Accepted

(a)

(b)

(c)

(d) (Accepted) (AD = 1.7713)

(e) (Accepted) (AD = 1.8534)

(f) (Accepted) (AD = 1.0155)
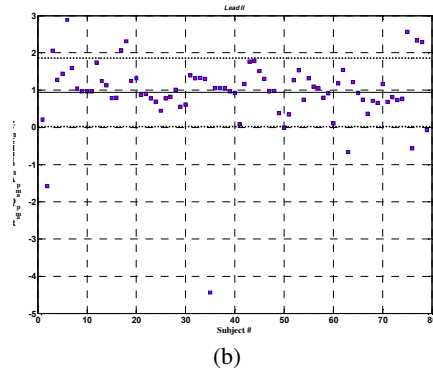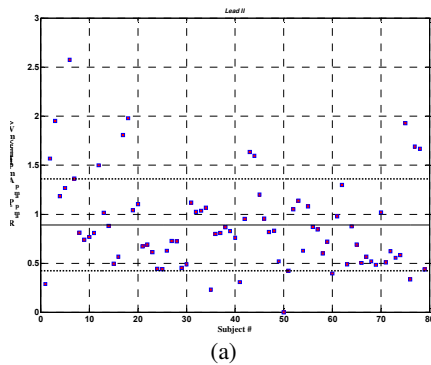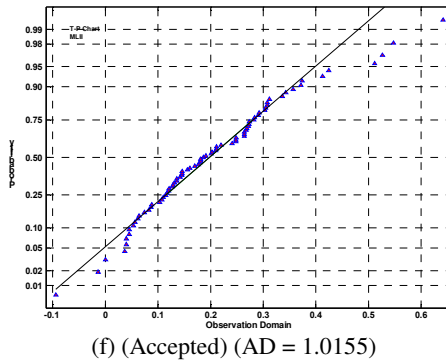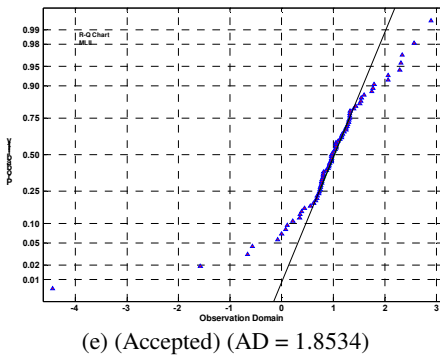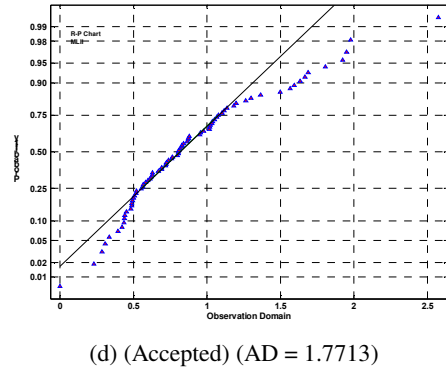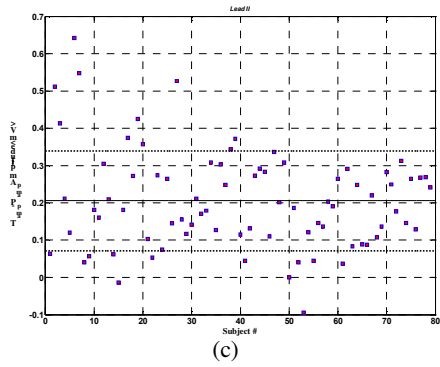
Fig. 2. (a,b,c): Dispersion of the data obtained from the wave amplitude difference calculations in lead II. The solid and dashed lines represent the mean value, $\mu - \sigma$ and $\mu + \sigma$ of the data, respectively.

(d,e,f): The probability $F(\mathbf{X} \le x)$ versus observation domain plot. The straight solid line represents the best line which can be fitted to the probabilities. The triangles illustrate the calculated probabilities. The normality test will be rejected in the cases that the triangles are far from the straight line or show high curvature.

(a)

(b)

(c)

(d) (Accepted) (AD = 2.0346)
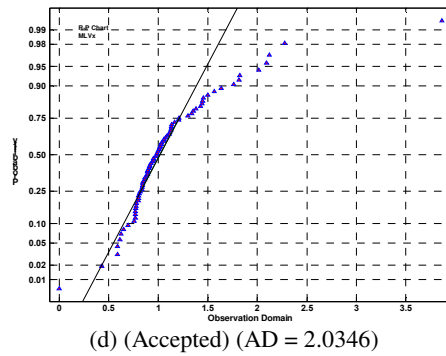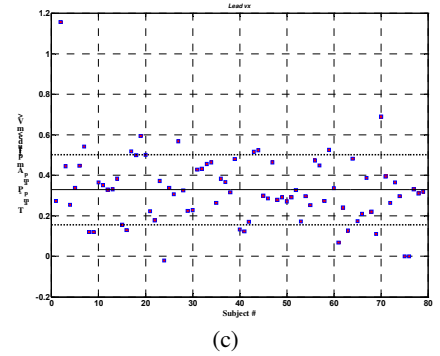
(e) (Accepted) (AD = 1.9321)   (f) (Accepted) (AD = 1.0167)

Fig. 3. (a,b,c): Dispersion of the data obtained from the wave amplitude difference calculations in lead V_x. The solid and dashed lines represent the mean value, $\mu - \sigma$ and $\mu + \sigma$ of the data, respectively.
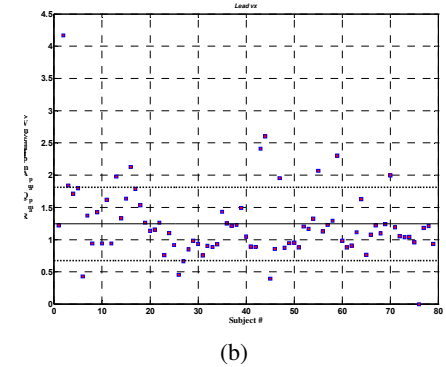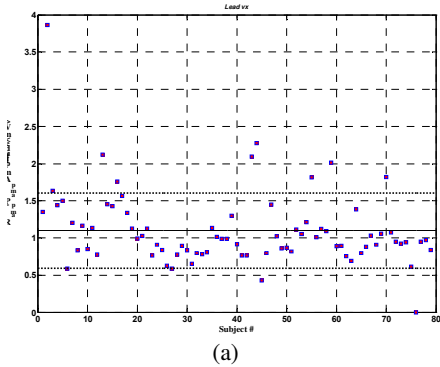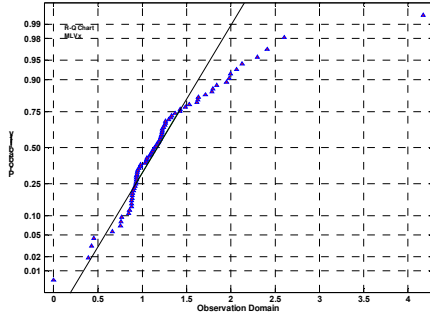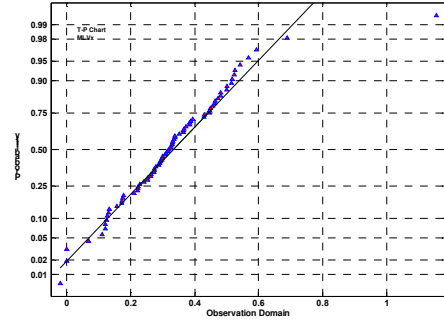
(d,e,f): The probability $F(X \le x)$ versus observation domain plot. The straight solid line represents the best line which can be fitted to the probabilities. The triangles illustrate the calculated probabilities. The normality test will be rejected in the cases that the triangles are far from the straight line or show high curvature.

2.2 Discussion

Regarding the performed statistical analyses, it can be seen that for differences T-P, R-Q and R-P, according to the ADDT, there are approximately 14.3% cases among all leads that fail the normality test. It is obvious that the normality test rejection (NTR) percent has inverse proportion to the threshold τ. Loosely speaking, if threshold τ is chosen a large number say 4, most of the A/B ratios will remain under the threshold. Thus, NTR will tend to zero and consequently test does not reject the normality hypothesis. For ADDT, if threshold τ is chosen to be $1.2 \le \tau \le 2.5$, acceptable results would be expected from the test, [13]. In this study, by selecting $\tau = 2.2$, it is shown that approximately 85.7% of all aforementioned differences, suitably pass the ADDT. This result can satisfactorily be generalized and applied to the remained differences omitted to appear in this study. It should be noted that according to the Central Limit Theorem (CLT), [13], if the number of samples chosen from random population is large enough, behavior of the selected population can be expected to be normal. Accordingly, due to sufficient number of subjects studied in this paper, the behavior of most of the differences will approximately be close to the normal distribution. Implementing the fact that the ADDT illustrates normal behavior of differences in most of the leads, the structure of appropriate estimators can be designed on the basis of various strategies. As a case in view, in this study it is assumed that the amplitude of the P-wave in lead I is measured and the amplitudes of the remaining waves in the same lead and the other leads are estimated by applying the proper estimator. Therefore, with the aid of this method a useful tool can be designed using which different electrical pictures of the heart electrical activity can be obtained. So far, numerous algorithms have been designed and developed based upon the finite element methods, [20], to generate such electrical pictures. Although acceptable results can be gained using these algorithms in normal cases and some arrhythmias; however, they have their own specific limitations. The major advantage of the presented model of our study is that it almost has no limitation in the generation of the artificial ECG signals. It will be demonstrated that how complicated arrhythmias can be generated using this model.

3 Description of the Algebraic Model of Artificial ECG Generator

The presented mathematical model is based on the idea that the overall generated artificial signal is developed by the superposition of some events with least similarities in their domains. Indeed, the amplitude of event k has no effect on the amplitude of the events $k-1$ and $k+1$, unless these two events are significantly close to each other. The studies conducted in this field indicate the fact that electrocardiogram waves generated due to the heart depolarization (i.e. P-wave and QRS complex) will have rather symmetric morphologies; however, the repolarization waves such as T-wave will be asymmetric on the skin surface due to the impulsive and asymmetric morphology of the action potential on the epicardial surface [1, 20, 21]. Accordingly, assume that the event i in the electrocardiogram signal of the lead j and heart beat k is defined as

$$E_{ij}(k,s) = C_{ij}(k)\exp\left[\frac{-1}{2\sigma_{ij}^2(k)}\left(s_j(k)-\mu_{ij}(k)\right)^2\right] \quad (10)$$

where C_{ij}, σ_{ij}, μ_{ij} are the corresponding parameters of the event E_{ij} and should be determined as to the event

could be generated using the arbitrary amplitude, incidence time, and duration. According to the Eq. 10, it is obvious that the function $E_{ij}(s)$ has a single extremum value of C_{ij} at $s = \mu_{ij}$. Thus, C_{ij} and μ_{ij} will represent the incidence amplitude and incidence time along the s-axis, respectively. In order to evaluate the duration of event $E_{ij}(s)$, the event start point is illustrated by s_{ON}^{ij} and the end point is depicted with s_{OFF}^{ij}. It is supposed that function $E_{ij}(s)$ has an infinitesimal positive value of ε in the position s_{ON}^{ij} or s_{OFF}^{ij}. Therefore,

$$
\varepsilon = C_{ij}(k)\exp\left[\frac{-1}{2\sigma_{ij}^2(k)}\left(s_{ij}^{OFF}(k) - \mu_{ij}(k)\right)^2\right]
$$
$$
\Rightarrow \frac{-1}{2\sigma_{ij}^2(k)}\left(s_{ij}^{OFF}(k) - \mu_{ij}(k)\right)^2 = \qquad (11)
$$
$$
\ln\left(\frac{\varepsilon}{\left|C_{ij}(k)\right|}\right)
$$

If half of the duration of the event $E_{ij}(s)$ is equal to $\xi_{ij}(k) = s_{OFF}^{ij}(k) - \mu_{ij}(k)$, then

$$
s_{ij}^{OFF} - \mu_{ij}(k) = \xi_{ij}(k)
$$
$$
\Rightarrow \frac{-1}{2\sigma_{ij}^2(k)} = \frac{1}{\xi_{ij}^2(k)}\ln\left(\frac{\varepsilon}{\left|C_{ij}(k)\right|}\right) \qquad (12)
$$
$$
= -\lambda_{ij}^2(k)
$$

and the Eq. 10 can be re-written as:

$$
E_{ij}(k,s) =
$$
$$
C_{ij}(k) \times
$$
$$
\exp\left[-\lambda_{ij}^2(k)\left(s_j(k) - \mu_{ij}(k)\right)^2\right] \qquad (13)
$$

Consequently, with the values of the parameters C_{ij}, λ_{ij}, μ_{ij} known, the amplitude, duration and incidence time for the event $E_{ij}(s)$ will be determined independently. The superposition of these events can be a good approach to the development of an exhaustive set of all waveforms in the lead j, as follows

$$
E_j(s) = \bigcup_{k=1}^{N_B}\left\{\bigcup_{i=1}^{N_j}\left\{E_{ij}(k,s)\right\}\right\}
$$
$$
= \bigcup_{k=1}^{N_B}\left\{\sum_{i=1}^{N_j}C_{ij}(k)\exp\left[-\lambda_{ij}^2(k)\left(s_j(k) - \mu_{ij}(k)\right)^2\right]\right\} \qquad (14)
$$

where $C_{ij}(k)$ and $\mu_{ij}(k)$ represent the incidence amplitude and incidence time of the k-th beat along the s-axis, respectively. Note that the index ij indicates event i in the lead j. $\lambda_{ij}(k)$ is i-th event in j-th lead duration parameter that if is chosen according to Eq. (12), desired duration will be obtained. In Eq. (14), it is assumed that the independent variable $s_j(k)$ is an arc length of a circle with an origin in $\theta = 0$, and when $\theta = \omega t$, it will be equal to $s = r\omega t$ (see Fig. 4). It should also be mentioned that all events in a heartbeat will occur in a complete revolution on the circle. Therefore, with a heart period of τ for a complete heartbeat, the circular frequency for the revolution on a circle with radius r will equal $\omega = \frac{2\pi}{\tau}$. Given the values of the parameters $C_{ij}(k)$, $t_{ij}^\mu(k)$ and $t_{ij}^\xi(k)$ by the user, the parameter values of $\lambda_{ij}(k)$ and $\mu_{ij}(k)$ in Eq. 10 for the event i in the lead j can be obtained from the following equation

$$
\begin{cases}
\mu_{ij}(k) = r\,\omega t_{ij}^\mu(k), \\[2mm]
\xi_{ij}(k) = r\,\omega t_{ij}^\xi(k) \Rightarrow \\[2mm]
-\lambda_{ij}^2(k) = \dfrac{1}{\xi_{ij}^2(k)}\ln\left(\dfrac{\varepsilon}{\left|C_{ij}(k)\right|}\right)
\end{cases} \qquad (15)
$$

3.1 Adding Transient ST Segment Episodes to the Algebraic Model

With the aim of modeling the effects of transient ST-episodes (TSE), an event with three distinct parts is considered in this section. The beginning and last parts are each consisting of the half of the Eq. 10 function, and a straight line with a positive, negative, or zero slope will connect these two parts. Therefore, a TSE wave will be characterized by 6 parameters, namely as $\xi_{ij}'(k)$, $\xi_{ij}''(k)$, $C_{ij}'(k)$, $m_{ij}'(k)$, $\mu_{ij}'(k)$, $\mu_{ij}''(k)$, which are schematically illustrated in Fig. 5. The ascending and descending rate of the ST-segment can be adjusted using the parameter $m_{ij}'(k)$. With the values of the parameters $\mu_{ij}'(k)$ and $\mu_{ij}''(k)$ equal to each other, an asymmetric T-wave, which is close to reality [12], will be generated.

3.2 Adding Heart Rate Variability (HRV) to the Algebraic Model

The artificial RR-tachogram algorithm developed by McSharry-Clifford, 2003 [5], is implemented in this study in order to include the effect of HRV in the presented algebraic model. In their model, RR-tachogram could be generated with the adjustment of

the power spectrum of RR time series using fast Fourier Transform (FFT) and inverse Fourier Transform [5, 14]. In this study, the power spectrum of RR time series in rest position is approximated with VLF/LF and HF/LF power ratios and the resulted RR sequence is added to the algebraic model. In order to adjust the RR distances in the algebraic model, suppose that $RR_j(k)$ represents the distance between two subsequent R-peaks in the heartbeats k-1 and k. Also assume that the time period of the complete heartbeat k in the lead j is equal to $\tau_j(k)$.

If so, the position of all R-peaks can be obtained from the following recursive equation. For the value $i = R$, $t_{ij}^\mu(k)$ represents the position of peak R in the beat k

$$\begin{cases} t_{ij}^\mu(k) = t_{ij}^\mu(k) + RR_j(k-1) \\ i = R \end{cases} \quad (16)$$

If the end point of the beat k in the lead j is illustrated by $EP_j(k)$, then $\tau_j(k)$ can be calculated from the following equation

$$\begin{cases} t_{ij}^\mu(k) - EP_j(k) = t_{ij}^\mu(1) \times \tau_j(k) \\ i = R \end{cases} \quad (17)$$

$$\begin{cases} \tau_j(k) = \dfrac{t_{ij}^\mu(k) - EP_j(k)}{t_{ij}^\mu(1)} \\ i = R \end{cases} \quad (18)$$

Finally, the following recursive equation can be used for the calculation of the end point of the beat k

$$EP_j(k) = EP_j(k-1) + \tau_j(k) \quad (19)$$

Solving the Eqs. 15 to 19, the end point of each heartbeat can be obtained as a function of instantaneous artificial heart rate, as to the time sequence $RR_j(k)$ will be similar to the artificial values. Modulation of the QRS complexes using the presented algorithm is illustrated in Fig. 6. The effect of respiration is added to the model using a sinusoid signal with certain amplitude and frequency. A normal additive noise with the mean value of zero and variance $\sigma^2 = 10^{-6}$ is also added to the model as the measurements noise in order to increase the similarity of the model to the actual signals.
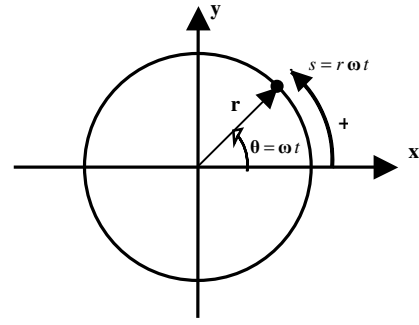
Fig. 4. The definition of the variable $s = r\omega t$ and its positive direction. It is assumed that an object with the angular velocity ω moves on a circle with the radius r
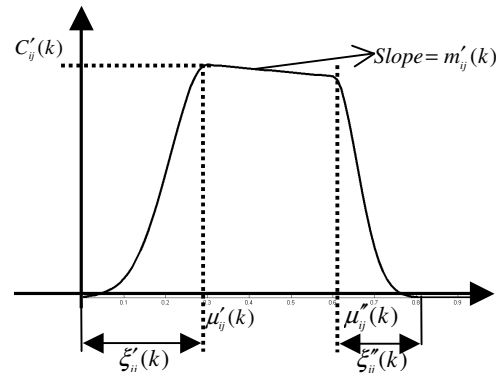
Fig. 5. Representation of the transient ST-segment Episodes (TSE). Each TSE is specified by 6 parameters $\xi_{ij}'(k)$, $\xi_{ij}''(k)$, $C_{ij}'(k)$, $m_{ij}'(k)$, $\mu_{ij}'(k)$, $\mu_{ij}''(k)$, and can have a positive, negative, or zero slope.
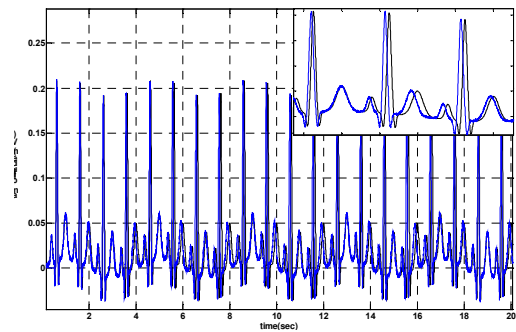
Fig. 6. Modulation of QRS complexes based on Eq.s 17 to 19 using artificial RR-tachogram generator introduced in [9]

3.3 Design of Bayesian Estimator of WaveAmplitude Algebraic Model

In section B it was shown that the differences between the waves amplitudes can be cast in a probabilistic framework. Thus, it will determine the estimator structure after the selection of estimation strategy. In this study, we have used the idea that the

probability density function of the P-wave amplitude in the lead I is determined using statistical analyses and the amplitude of all other waves in the same lead and other leads can then be determined with the observation of the P-wave amplitude in the lead I.

It should be noted that there is a wide definition for the expression of normality (healthy) in the medical terminology (for instance a "normal" fat smoker and a "normal" young athlete). Therefore, the designed estimator will not be capable to present precise results. The reasonable, but not accurate, predictions of the presented model using the collected data is the most significant point of the presented strategy.

Assume the random variable $\mathbf{X}$ defined in the domain $\mathbf{\Omega}$, i.e. $\{p_\mathbf{X}; x \in \mathbf{\Omega}\}$ where $p_\mathbf{X}$ is the probability density function for $\mathbf{X} = x$, specifies a family of distributions for the random observation $\mathbf{Y}$. Also, suppose that the random observation $\mathbf{Y}$ has the values y defined in the domain $\mathbf{\Gamma}$. It is aimed to determine a mapping like $\hat{x}: \mathbf{\Gamma} \to \mathbf{\Omega}$ as to $\hat{x}(y)$ be the best guess for random variable $\mathbf{X}$ for the observed value $\mathbf{Y} = y$. To meet this end, a cost function of $C: \mathbf{\Omega} \times \mathbf{\Omega} \to \mathbf{R}$ is defined, in which $C[\hat{x}(y), x]$ is the imposed cost of the estimation of the actual value of the random variable $\mathbf{X}$ with the value $\hat{x}(y)$. If so, cost average over $\mathbf{Y}$ for each $x \in \mathbf{\Omega}$ can be defined as follows, [17],

$$R_x(\hat{x}) = E\left\{C[\hat{x}(\mathbf{Y}), x] \big| \mathbf{X} = x\right\} \qquad (20)$$

Regarding this equation, the Bayesian Risk which is in fact the mean value of the cost average $R_x(\hat{x})$ can be described as

$$\begin{aligned} &r_B(\hat{x}) = E\{R_\mathbf{X}(\hat{x})\} \Rightarrow \\ &r_B(\hat{x}) = E\{C[\hat{x}(\mathbf{Y}), \mathbf{X}]\} \\ &= E\{E\{C[\hat{x}(\mathbf{Y}), \mathbf{X}] | \mathbf{Y}\}\} \end{aligned} \qquad (21)$$

Accordingly, the Bayesian estimation of the random variable $\mathbf{X}$ for each value $y \in \mathbf{\Gamma}$ can easily be found by the minimization, if it exists, of the following posterior cost

$$E\left\{C[\hat{x}(y), \mathbf{X}] \big| \mathbf{Y} = y\right\} \qquad (22)$$

If the random variable $\mathbf{X}$ has the probability density $p_{\mathbf{X}|y}(x|y)$ for each $\mathbf{Y} = y$, $y \in \mathbf{\Gamma}$, then the Bayesian estimation $\hat{x}(y)$ for each value $y \in \mathbf{\Gamma}$ can be determined from the following equation

$$I_{pr} = \int_\mathbf{\Omega} C[\hat{x}(y), x] p_{\mathbf{X}|y}(x|y) \, dx \qquad (23)$$

In order to achieve the Minimum Mean Square Error (MMSE) estimation, the cost function $C[\hat{x}(y), x]$ is defined as follows

$$C[\hat{x}(y), x] = (\hat{x}(y) - x)^2 \qquad (24)$$

Since this cost function measures the estimator performance in terms of error square, it can be implemented in many cases and the resulted estimation will also have a closed form [17]. If so, the Bayesian estimator will be an MMSE estimator and the posterior cost for $\mathbf{Y} = y$ will be equal to

$$\begin{aligned} &E\left\{[\hat{x}(y) - \mathbf{X}]^2 \big| \mathbf{Y} = y\right\} = E\left\{[\hat{x}(y)]^2 \big| \mathbf{Y} = y\right\} \\ &- 2E\left\{\hat{x}(y)\mathbf{X} \big| \mathbf{Y} = y\right\} + E\left\{\mathbf{X}^2 \big| \mathbf{Y} = y\right\} \\ &= [\hat{x}(y)]^2 - 2\hat{x}(y) E\left\{\mathbf{X} \big| \mathbf{Y} = y\right\} \\ &+ E\left\{\mathbf{X}^2 \big| \mathbf{Y} = y\right\} \end{aligned} \qquad (25)$$

As can be observed, the above equation is a quadratic function of $\hat{x}(y)$ and can be re-written as follows

$$\begin{aligned} &E\left\{[\hat{x}(y) - \mathbf{X}]^2 \big| \mathbf{Y} = y\right\} = \\ &\left\{\hat{x}(y) - E\{\mathbf{X} | \mathbf{Y} = y\}\right\}^2 \\ &- [E\{\mathbf{X} | \mathbf{Y} = y\}]^2 + E\{\mathbf{X}^2 | \mathbf{Y} = y\} \end{aligned} \qquad (26)$$

This expression will have its minimum value if the complete square expression controlled by $\hat{x}(y)$ is equal to zero. Indeed

$$\begin{aligned} &\frac{\partial}{\partial \hat{x}(y)} E\left\{[\hat{x}(y) - \mathbf{X}]^2 \big| \mathbf{Y} = y\right\} = 0 \\ &\Rightarrow \hat{x}(y) = E\{\mathbf{X} | \mathbf{Y} = y\} \end{aligned} \qquad (27)$$

Solution of this equation will lead to a point in which the cost function achieves its unique minimum and the derivative of the cost function with respect to $\hat{x}(y)$ is equal to zero.

The MMSE estimation will consequently be the average conditional value of the random variable $\mathbf{X}$ for $\mathbf{Y} = y$. Thus, the random variable $\mathbf{X}$ should be averaged as follows

$$\hat{x}(y) = E\{\mathbf{X} | \mathbf{Y} = y\} \qquad (28)$$

If so, it is necessary to obtain a posterior conditional density ($p_{\mathbf{X}|y}(x|y)$) of the likelihood function ($p_{\mathbf{Y}|x}(y|x)$) using the following theorem:

Lemma 3: If $p_{\mathbf{Y}|x}(y|x)$ represents the conditional density (likelihood function), and random variables $\mathbf{X}$ and $\mathbf{Y}$ have marginal density functions $p_\mathbf{X}(x)$ and $p_\mathbf{Y}(y)$ respectively, then a posteriori density function, $p_{\mathbf{X}|y}(x|y)$ can be obtained from the following equation, [22]

$$p_{\mathbf{X}|y}(x|y) = \frac{p_{\mathbf{Y}|x}(y|x)\,p_{\mathbf{X}}(x)}{p_{\mathbf{Y}}(y)} \qquad (29)$$

$$p_{\mathbf{Y}}(y) = \int_{\Omega} p_{\mathbf{Y}|x}(y|x)\,p_{\mathbf{X}}(x)\,dx$$

Proof:

If $F(\cdot)$ represents the Cumulative Distribution Function (CDF), then

$$F(x < \mathbf{X} \leq x + \Delta_1 | \mathbf{Y} = y)$$
$$= \lim_{\Delta_2 \to 0} F(x < \mathbf{X} \leq x + \Delta_1 | y < \mathbf{Y} \leq y + \Delta_2) \qquad (30)$$

$$F(\{x < \mathbf{X} \leq x + \Delta_1\} \cap \{y < \mathbf{Y} \leq y + \Delta_2\})$$
$$= F(y < \mathbf{Y} \leq y + \Delta_2 | x < \mathbf{X} \leq x + \Delta_1)\, F(x < \mathbf{X} \leq x + \Delta_1) \qquad (32)$$

$$F(x < \mathbf{X} \leq x + \Delta_1 | \mathbf{Y} = y) = \lim_{\Delta_2 \to 0} \frac{F(y < \mathbf{Y} \leq y + \Delta_2 | x < \mathbf{X} \leq x + \Delta_1)\, F(x < \mathbf{X} \leq x + \Delta_1)}{F(y < \mathbf{Y} \leq y + \Delta_2)}$$

If the numerator and denominator of the right hand side of the Eq. 31 is divided by Δ_2, then

$$F(x < \mathbf{X} \leq x + \Delta_1 | \mathbf{Y} = y) = \lim_{\Delta_2 \to 0} \frac{\dfrac{F(y < \mathbf{Y} \leq y + \Delta_2 | x < \mathbf{X} \leq x + \Delta_1)}{\Delta_2} F(x < \mathbf{X} \leq x + \Delta_1)}{\dfrac{F(y < \mathbf{Y} \leq y + \Delta_2)}{\Delta_2}} \qquad (33)$$

Also, if both sides of the Eq. 33 are divided by Δ_1 and both Δ_1 and Δ_2 are tended to zero, i.e. $\Delta_1 \to 0, \Delta_2 \to 0$, then

$$\lim_{\Delta_1 \to 0} \frac{F(x < \mathbf{X} \leq x + \Delta_1 | \mathbf{Y} = y)}{\Delta_1} = \lim_{\Delta_1 \to 0} \left\{ \lim_{\Delta_2 \to 0} \frac{\dfrac{F(y < \mathbf{Y} \leq y + \Delta_2 | x < \mathbf{X} \leq x + \Delta_1)}{\Delta_2}}{\dfrac{F(y < \mathbf{Y} \leq y + \Delta_2)}{\Delta_2}} \frac{F(x < \mathbf{X} \leq x + \Delta_1)}{\Delta_1} \right\} \qquad (34)$$

According to the definition of the conditional density function in terms of conditional probability function [23] we have

$$p_{\mathbf{X}|y}(x|y) = \frac{p_{\mathbf{Y}|x}(y|x)\,p_{\mathbf{X}}(x)}{p_{\mathbf{Y}}(y)} \qquad (35)$$

On the other hand, if the conditional density $p_{\mathbf{Y}|x}(y|x)$ and the marginal density $p_{\mathbf{X}}(x)$ are both at hand, the marginal density $p_{\mathbf{Y}}(y)$ will simply be calculated by integrating Eq. 32 as follows

$$p_{\mathbf{X}|y}(x|y) = \frac{p_{\mathbf{Y}|x}(y|x)\,p_{\mathbf{X}}(x)}{p_{\mathbf{Y}}(y)} \qquad (36)$$

Because according to the Eq. 32, we can write

Using the conditional probability function [23] properties, the latter equation can be written as

$$F(x < \mathbf{X} \leq x + \Delta_1 | y < \mathbf{Y} \leq y + \Delta_2)$$
$$= \frac{F(\{x < \mathbf{X} \leq x + \Delta_1\} \cap \{y < \mathbf{Y} \leq y + \Delta_2\})}{F(y < \mathbf{Y} \leq y + \Delta_2)} \qquad (31)$$

and the right side of the Eq. 31 will be as follows

$$p_{\mathbf{XY}}(x, y) = p_{\mathbf{Y}|x}(y|x)\,p_{\mathbf{X}}(x) \qquad (37)$$

and this is the end of the proof. Therefore, using the Eqs. 28 and 36, $\hat{x}_{MMSE}(y)$ can be derived from the following equation

$$\hat{x}_{MMSE} = E\{\mathbf{X} | \mathbf{Y} = y\} =$$
$$\int_{\Omega} x\, p_{\mathbf{X}|y}(x|y)\,dx$$
$$= \frac{\int_{\Omega} x\, p_{\mathbf{Y}|x}(y|x)\,p_{\mathbf{X}}(x)\,dx}{\int_{\Omega} p_{\mathbf{Y}|x}(y|x)\,p_{\mathbf{X}}(x)\,dx} \qquad (38)$$

Assume $\mathbf{X}$ and $\mathbf{Y}$ to be two random variables, where $\mathbf{X}$ is a normal random variable with the density $N(\mu_x, \sigma_x^2)$ and the random variable $\mathbf{Y} - \mathbf{X}$ has the

normal pdf $N(\mu_0, \sigma_0^2)$. The likelihood density function will then have the normal density pdf $N(\mu_0 + x, \sigma_0^2)$ for $\mathbf{X} = x$ and we have

$$(\mathbf{Y} - \mathbf{X}) \sim N(\mu_0, \sigma_0^2) \tag{39}$$

$$\mathbf{X} \sim N(\mu_x, \sigma_x^2) \tag{40}$$

$$\mathbf{Y}\big|_{\mathbf{X}=x} \sim N(\mu_0 + x, \sigma_0^2)$$
$$= \frac{1}{\sqrt{2\pi}\sigma_0} \exp\left(-\frac{1}{2\sigma_0^2}(y - \mu_0 - x)^2\right) \tag{41}$$

According to the Eq. 38, the $\hat{x}_{MMSE}(y)$ estimation using the observation y will be as follows

$$\hat{x}_{MMSE}(y) = \frac{\int_\Omega x \frac{1}{\sqrt{2\pi}\sigma_0} \exp\left(-\frac{1}{2\sigma_0^2}(y-\mu_0-x)^2\right) \frac{1}{\sqrt{2\pi}\sigma_x} \exp\left(-\frac{1}{2\sigma_x^2}(x-\mu_x)^2\right) dx}{\int_\Omega \frac{1}{\sqrt{2\pi}\sigma_0} \exp\left(-\frac{1}{2\sigma_0^2}(y-\mu_0-x)^2\right) \frac{1}{\sqrt{2\pi}\sigma_x} \exp\left(-\frac{1}{2\sigma_x^2}(x-\mu_x)^2\right) dx} \tag{42}$$

which can be simplified to the following equation

$$\hat{x}_{MMSE}(y) = \frac{\int_{-\infty}^{+\infty} x \exp\left(-\frac{1}{2\sigma_0^2}(y-\mu_0-x)^2 - \frac{1}{2\sigma_x^2}(x-\mu_x)^2\right) dx}{\int_{-\infty}^{+\infty} \exp\left(-\frac{1}{2\sigma_0^2}(y-\mu_0-x)^2 - \frac{1}{2\sigma_x^2}(x-\mu_x)^2\right) dx} \tag{43}$$

In the Eq. 43, the values of the integrals in numerator and denominator should be computed for $\mathbf{Y} = y$ in order to obtain the value of $\hat{x}_{MMSE}(y)$. However, analytical solution of these integrals is a hard and tedious task and certain numerical methods can be implemented. In the Fig. 7, $\hat{x}_{MMSE}(y)$ is illustrated for $\mu_x = \mu_0 = 0$ in three cases of $y = 0, y < 0$, and $y > 0$. In Fig. 7, the lower surface illustrates the performance of the estimator of the Eq. 43 for $y = 0$, and σ_0, σ_x, variations in the $(0, 1.5)$ range. As can be observed, when $y = 0$, the estimation magnitude will be higher for an increase in σ_0 or σ_x. When $y \neq 0$,

and σ_x is very small, the upper part of Fig. 7, the best estimation will be equal to zero for all positive or negative observations. This result seems logical, because the infinitesimal value of σ_x will suggest a deterministic behavior for the random variable $\mathbf{X}$. However, for a great value of σ_x, there would be a decrease in the estimation magnitude relative to observation when σ_0 increases. This is due to the fact that an increase in σ_0, will result in an increase in the observations variance, and this causes the best estimation to be a very small value. For a high value of σ_0, the same justification as σ_x can be implemented.

Table 4. Parameters of normal ECG signal in lead avr

Parameters	Events			
	P	Q	R	T
$\mathbf{t}_{ij}^\mu$ <sec>	8.75	8.89	8.92	9.14
C_{ij} <mV>	-0.2	-1.0	0.1	-0.3
$\mathbf{t}_{ij}^\xi$ <sec>	0.1266	0.0448	0.0448	0.3250

Table 5. Parameters of normal ECG signal in lead V_1

Parameters	Events			
	P	R	S	T
$\mathbf{t}_{ij}^\mu$ <sec>	12.14	12.26	12.29	12.57
C_{ij} <mV>	-0.1	0.19	-1.11	-0.2
$\mathbf{t}_{ij}^\xi$ <sec>	0.1036	0.0448	0.0822	0.2622

Table 6. Parameters of normal ECG signal in lead V_3

Parameters	Events			
	P	R	S	T
$\mathbf{t}_{ij}^{\mu}$ <sec>	8.45	8.61	8.64	8.83
C_{ij} <mV>	0.2	0.97	-2.04	0.81
$\mathbf{t}_{ij}^{\xi}$ <sec>	0.1266	0.0448	0.0448	0.3921

Table 7. Parameters of normal ECG signal in lead V_6

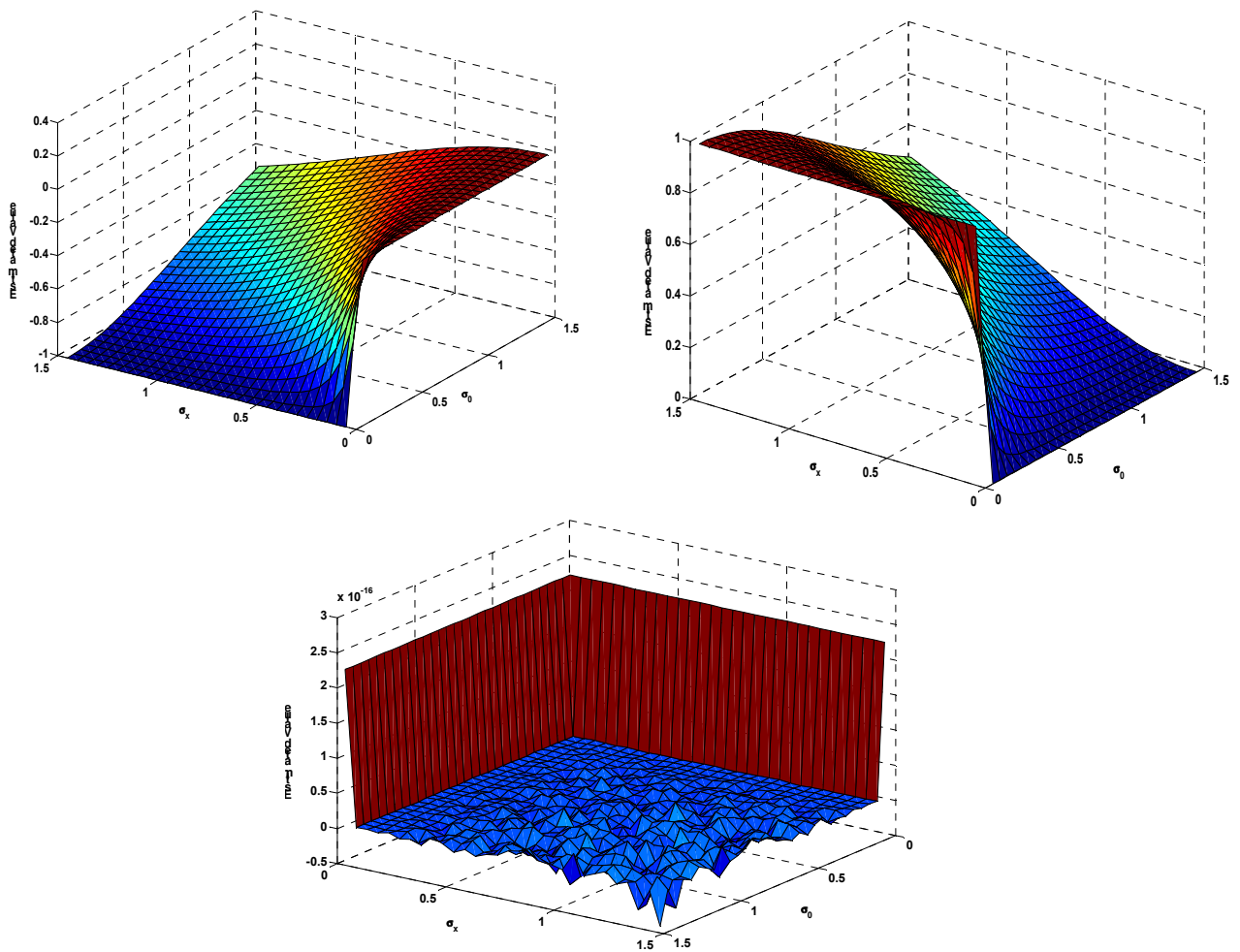| Parameters	Events				
	P	Q	R	S	T
$\mathbf{t}_{ij}^{\mu}$ <sec>	9.55	9.695	9.715	9.74	10
C_{ij} <mV>	0.05	-0.2	1.2	-0.4	0.5
$\mathbf{t}_{ij}^{\xi}$ <sec>	0.1769	0.0291	0.0448	0.0448	0.2041

Fig. 7. Bayesian Estimation of the random variable X based on normal observation $\mathbf{Y} = y$ describes by Eq. (42) (up-left), $y < 0$, (up-right), $y > 0$ and (bottom), $y = 0$

4   Simulation Results

The results of various simulations will be illustrated in this part.

4.1   15 Lead Normal ECG Generator (including Probable U-Waves)

First, the simulation method of generating 15-lead normal ECG signal with U-wave are presented. Some abnormal electrocardiographic phenomena are then simulated. In Figs. 8 to 11, a normal beat is shown in the leads AVR, V1, V3, and V6, respectively and the corresponding parameter values are presented in Tables 4 to 7. It should be noted that the lead AVR and V1 have no S-wave, and no Q-wave, respectively. However, the lead V6 contains all events. In Fig. 12, an

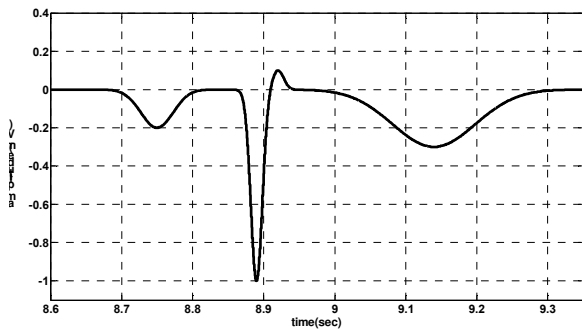example of a heart beat with a U-wave is depicted and the corresponding parameters are represented in Table 8.
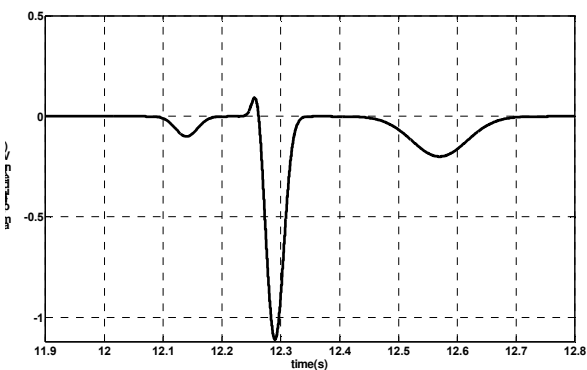

Fig. 8. Simulated normal ECG signal in lead avr

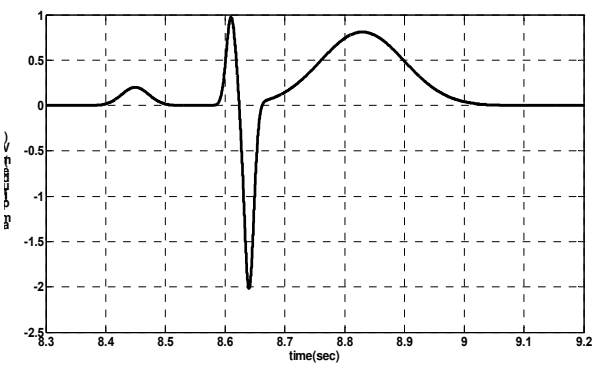**Fig. 9.** Simulated normal ECG signal in lead V_1

Fig. 10. Simulated normal ECG signal in lead V_3
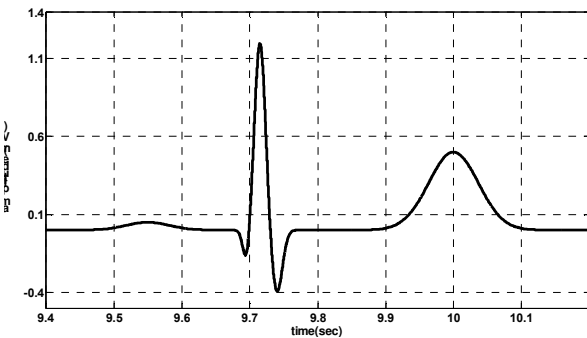
Fig. 11. Simulated normal ECG signal in lead V_6
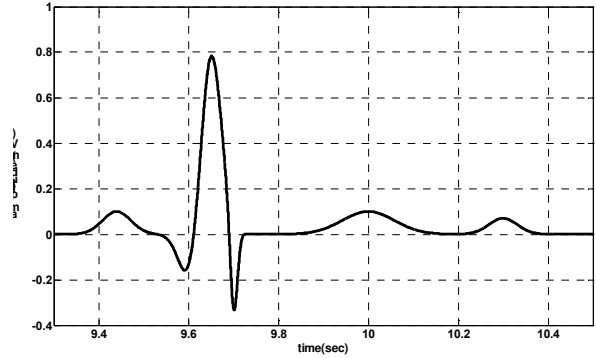
Fig. 12. Simulated normal ECG signal in lead I including U-wave

4.2 Fascicular Ventricular Tachycardia (Left Septal Ventricular Tachycardia)

A left septal Ventricular Tachycardia (VT) has been described as arising in the left posterior septum, often preceded by a fascicular potential, and is sometimes called a fascicular tachycardia (Fig. 13). The simulated abnormal left septal ventricular tachycardia waveforms are demonstrated in Figs. 14 to 17 and the corresponding parameter values are presented in Tables 9 to 12. The comparison of the simulated waveforms and real shapes of electrocardiographic signals (depicted in Fig. 13) indicates the high flexibility of the introduced model in generating artificial abnormal ECG waveforms.
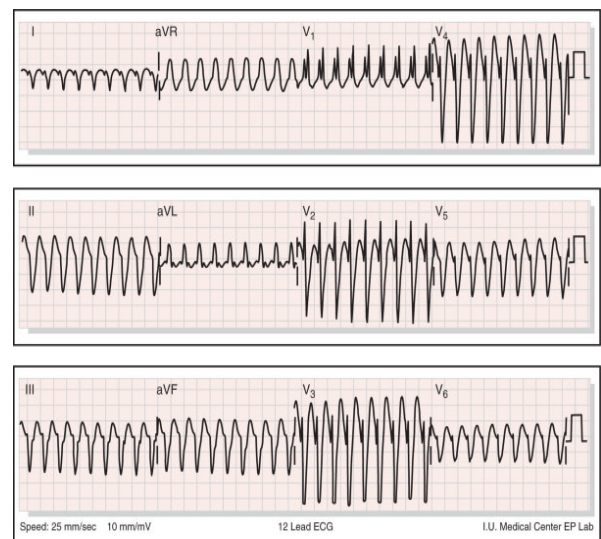
Fig. 13. Left septal ventricular tachycardia. This tachycardia is characterized by a right bundle branch block contour.
In this instance, the axis was rightward. The site of the ventricular tachycardia was established to be in the left posterior septum by electrophysiological mapping and ablation, adopted from [12]
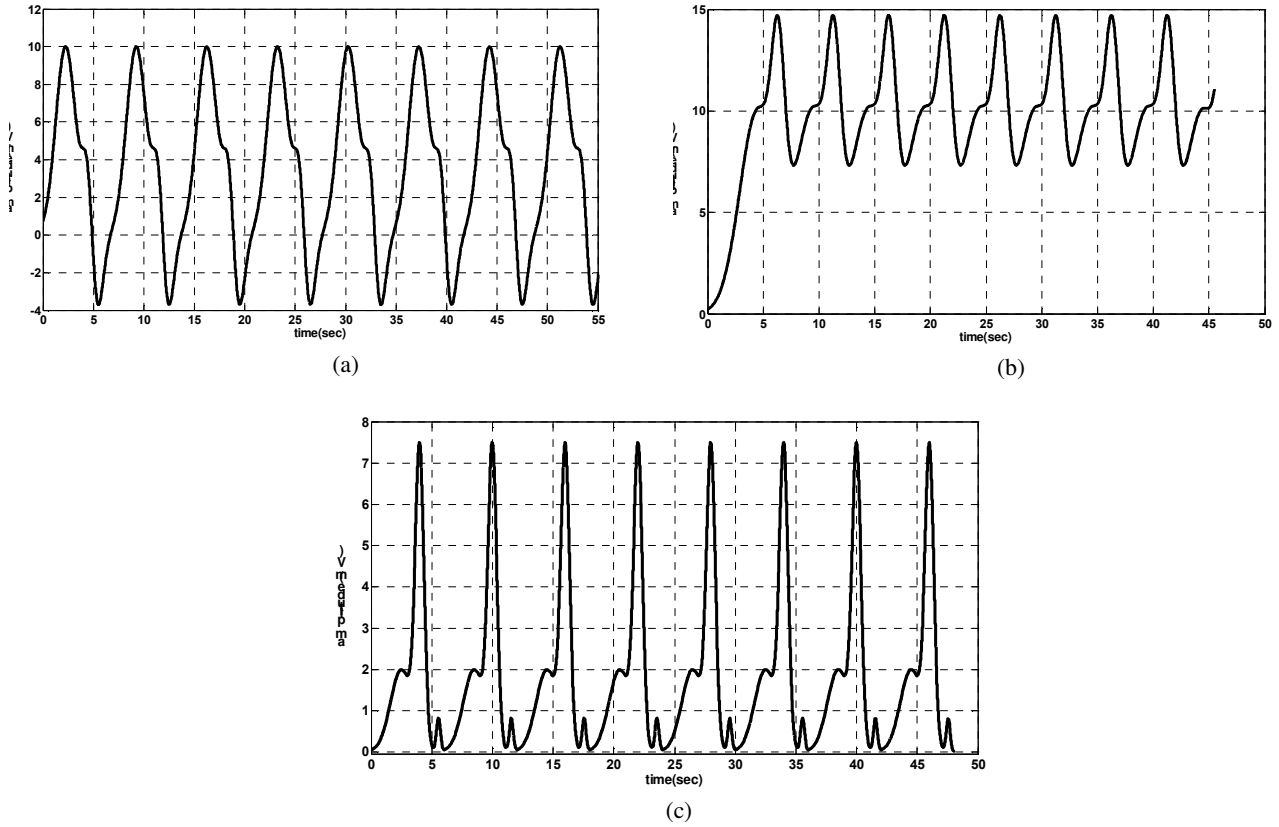
Fig. 14. Simulated left septal ventricular tachycardia in leads (a) avf, (b) avl, and (c) avr

Table 8. Parameters of normal ECG signal in lead I including U-wave

Parameters	Events					
	P	Q	R	S	T	U
$\mathbf{t}_{ij}^{\mu}$ <sec>	9.44	9.6	9.65	9.7	10	10.3
C_{ij} <mV>	0.1	-0.2	0.8	-0.4	0.1	0.07
$\mathbf{t}_{ij}^{\xi}$ <sec>	0.1769	0.1266	0.1266	0.0448	0.325	0.1769

Table 9. Parameters of left septal ventricular tachycardia in leads (a) avf, (b) avl, and (c) avr

Parameters	Events		
	P	Q	R
$\mathbf{t}_{ij}^{\mu}$ <sec>	-0.5	3	3.5
C_{ij} <mV>	10	5	-5
$\mathbf{t}_{ij}^{\xi}$ <sec>	5	6	7

(a)

Parameters	Events		
	P	Q	R
$\mathbf{t}_{ij}^{\mu}$ <sec>	0	3	5.1
$\mathbf{t}_{ij}^{\xi}$ <sec>	5	5	6
C_{ij} <mV>	2	7	0.8

(b)

Parameters	Events	
	P	Q
$\mathbf{t}_{ij}^{\mu}$ <sec>	0	4.7
$\mathbf{t}_{ij}^{\xi}$ <sec>	9	8
C_{ij} <mV>	10	8

(c)

Fig. 15. Simulated left septal ventricular tachycardia in leads (a) I, (b) II, and (c) III

Table 10. Parameters of left septal ventricular tachycardia in leads (a) I, (b) II, and (c) III

	Events	
Parameters	P	Q
$\mathbf{t}_{ij}^{\mu}$ <sec>	0	5
$\mathbf{t}_{ij}^{\xi}$ <sec>	9	8
C_{ij} <mV>	10	4.5

(a)

	Events		
Parameters	P	Q	R
$\mathbf{t}_{ij}^{\mu}$ <sec>	0	1.75	3.8
$\mathbf{t}_{ij}^{\xi}$ <sec>	3.5	5	7.4
C_{ij} <mV>	7	3	-12

(b)

	Events		
Parameters	P	Q	R
	0	4	4.5
$\mathbf{t}_{ij}^{\xi}$ <sec>	5.5	6	8
C_{ij} <mV>	7	2.3	-10

(c)

Table 11. Parameters of left septal ventricular tachycardia in leads (a) V_1, (b) V_2, and (c) V_3

	Events		
Parameters	P	Q	R
$\mathbf{t}_{ij}^{\mu}$ <sec>	-0.5	1.2	2.5
$\mathbf{t}_{ij}^{\xi}$ <sec>	2.8	3	4
C_{ij} <mV>	2	8	10

(a)

	Events		
Parameters	P	Q	R
$\mathbf{t}_{ij}^{\mu}$ <sec>	-2	5	6
$\mathbf{t}_{ij}^{\xi}$ <sec>	7	6	8
C_{ij} <mV>	5	12	-20

(b)

(a)

(b)

(c)
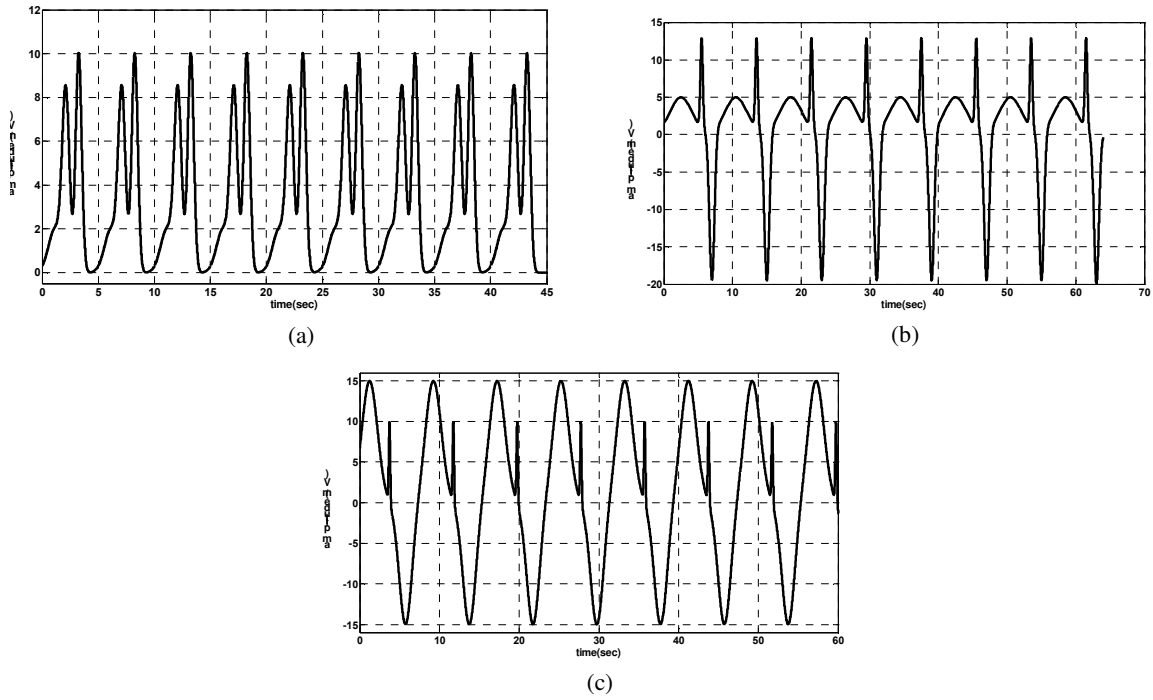
Fig. 16. Simulated left septal ventricular tachycardia in leads (a) V_1, (b) V_2, and (c) V_3
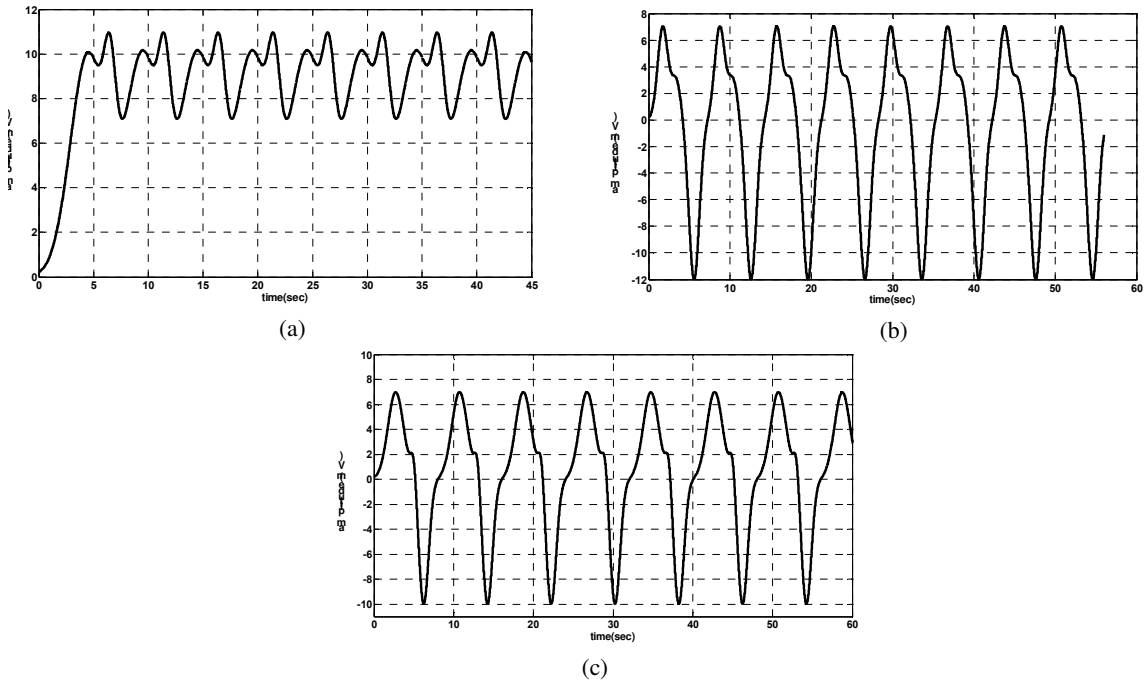

(a)

(b)

(c)
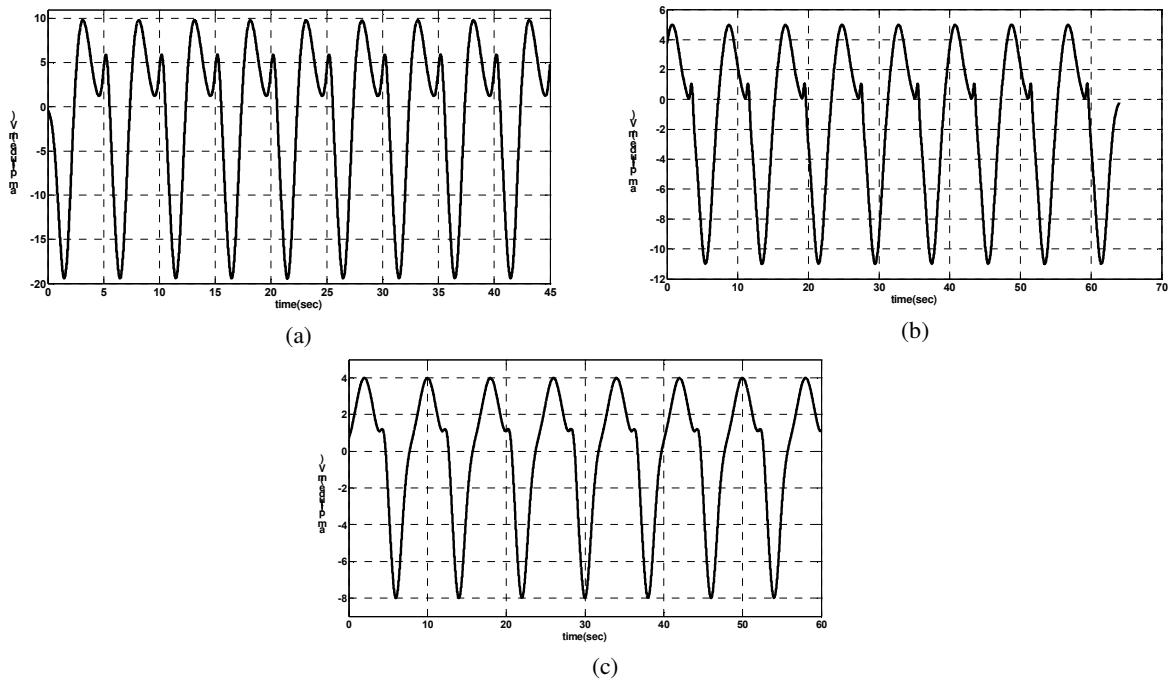
Fig. 17. Simulated left septal ventricular tachycardia in leads (a) V_4, (b) V_5, and (c) V_6

Table 12. Parameters of left septal ventricular tachycardia in leads (a) V_4, (b) V_5, and (c) V_6

Parameters	Events		
	P	Q	R
$\mathbf{t}_{ij}^{\mu}$ <sec>	0	1.2	4.5
$\mathbf{t}_{ij}^{\xi}$ <sec>	3	5	6
C_{ij} <mV>	-20	10	7

(a)

Parameters	Events		
	P	Q	R
$\mathbf{t}_{ij}^{\mu}$ <sec>	-2	3	2.9
$\mathbf{t}_{ij}^{\xi}$ <sec>	3.5	4	8
C_{ij} <mV>	5	2	-11

(b)

	Events		
Parameters	P	Q	R
$\mathbf{t}_{ij}^{\mu}$ <sec>	-1	3.5	4
$\mathbf{t}_{ij}^{\xi}$ <sec>	5	5.5	8
C_{ij} <mV>	4	1.5	-8

(c)

4.3 Rate-Dependent Conduction Blocks or Aberration (Tachycardia, Bradycardia)

Conduction delays in the intra-ventricular parts can be due to changes in heart rate, or pathological lesions in the conduction system. Rate-dependent block (aberration) can occur in relatively low or high heart rates. A very pervasive kind of rate-dependent block which has the electrocardiographic pattern of Right Bundle Branch Block (RBBB) or Left Bundle Branch Block (LBBB) is called acceleration (tachycardia)-dependent block, in which conduction delay happens when heart rate exceeds a specific critical threshold. On the other hand, in deceleration (bradycardia)-dependent block conduction delay takes place when heart rate is less than the specific critical threshold. Deceleration-dependent block is less prevalent in comparison to acceleration-dependent block and only occurs in patients with remarkable defect in the conduction system.

In Fig. 18-a, a sample acceleration-dependent QRS aberration is depicted. As can be seen in this picture, the duration of the basic cycle, C is equal to 760 milliseconds, and left bundle branch block (LBBB) occurs when C reaches the value of 700 milliseconds, which is annotated by some points. The occurred block will then continue with the cycle duration of 700msec in Fig. above and 840msec in Fig. below, which is annotated by arrowheads. Eventually, the conduction system returns to its normal conditions after a heart beat with duration of 600msec. The beginning of each cycle with normal duration is illustrated by letter S, [12]. A simulated sample of this phenomenon is represented in Fig. 18-b. It should be noticed that three parameter sets will be required in this case which will apply to the points C, arrowhead, and S, which can be seen in Tables 13 to 15.

Fig. 18. (a) Electrocardiographic pattern of acceleration-dependent QRS aberration, adopted from [12], (b) the simulated signal with similar features

Table 13. parameters of acceleration-dependent aberration, phase I

Parameters	Events					
	P	Q	R	S	S'	T
$\mathbf{t}_{ij}^{\mu}$ <sec>	0.2150	0.3375	0.3950	0.4125	0.5450	0.7150
C_{ij} <mV>	0.7	-0.4	0.8	-0.7	0.6	0.6
$\mathbf{t}_{ij}^{\xi}$ <sec>	0.0850	0.0375	0.0650	0.0375	0.0850	0.0850

Table 14. Parameters of acceleration-dependent aberration, phase II

Parameters	Events			
	Q	S	T	T'
$\mathbf{t}_{ij}^{\mu}$ <sec>	0.2950	0.4500	0.7100	0.7250
C_{ij} <mV>	-0.8	-0.11	0.3	0.1
$\mathbf{t}_{ij}^{\xi}$ <sec>	0.1050	0.050	0.1900	0.0750

Table 15. Parameters of acceleration-dependent aberration, phase III

Parameters	Events		
	Q	S	S'
$\mathbf{t}_{ij}^{\mu}$ <sec>	0.2750	0.3500	0.4000
C_{ij} <mV>	-0.6	-0.6	-0.8
$\mathbf{t}_{ij}^{\xi}$ <sec>	0.0250	0.0500	0.1000

In Fig. 19-a, an example of deceleration-dependent aberration is presented. The basic rhythm is sinus rhythm with a Wenckebach (type I) atrioventricular (AV) block. With 1:1 AV conduction, the QRS complexes are normal in duration; with a 2:1 AV block or after the longer pause of a Wenckebach sequence, left bundle branch block (LBBB) appears, [12]. A simulated sample of this phenomenon is represented in Fig. 19-b. It should be noticed that two parameter sets will be required in this case (see Tables 16 and 17).

(a)

(b)

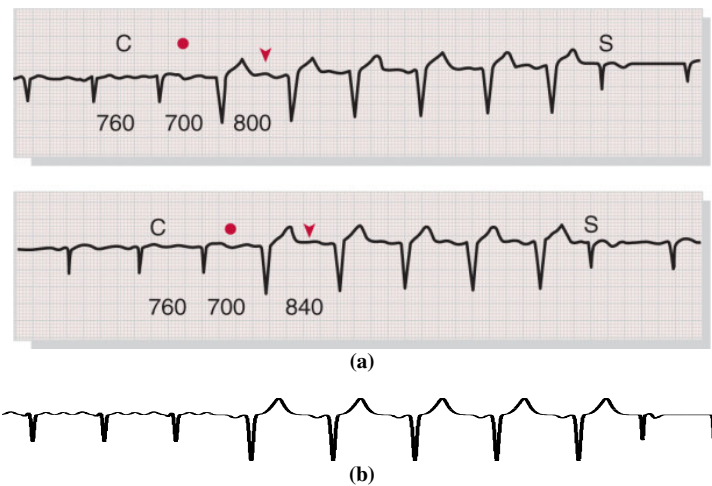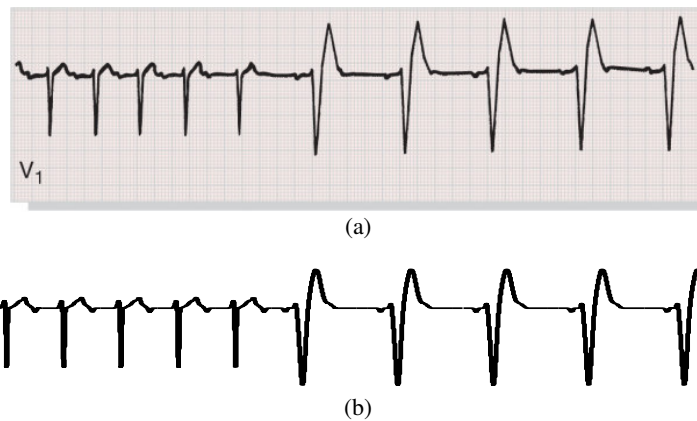**Fig. 19.** (a) Electrocardiographic pattern of deceleration-dependent aberration, [12]. (b) the simulated signal with similar features

Table 16. Parameters of deceleration-dependent aberration, phase I

Parameters	Events				
	P	Q	R	R'	S
$\mathbf{t}_{ij}^{\mu}$ <sec>	0.5	0.55	0.9500	1.025	1.3
C_{ij} <mV>	0.02	-0.16	0.02	0.01	-0.01
$\mathbf{t}_{ij}^{\xi}$ <sec>	0.1	0.0500	0.3500	0.0750	0.1

Table 17. Parameters of deceleration-dependent aberration, phase II s

Parameters	Events				
	P	Q	R	S	T
$\mathbf{t}_{ij}^{\mu}$ <sec>	0.35	0.625	0.8000	1.1500	1.5000
C_{ij} <mV>	-0.1	0.2	-2	1	0.1
$\mathbf{t}_{ij}^{\xi}$ <sec>	0.1	0.0750	0.2000	0.3500	0.2000

4.4 Acute Q- Wave Infarctions of anteriorlateral and inferior walls

Approximate classification and variability of electrocardiographic patterns of acute myocardial ischemia are illustrated in Fig. 20. It should be noted that this classification cannot be applied to all cases. As a case in view, a Q-wave infarct can evolve to a Q-wave infarct and an ST-elevation can be developed by a non-Q wave infarct. Reversely, ST- segment depression and T-wave inversion can occur by the happening of a Q-wave infarct, [12].
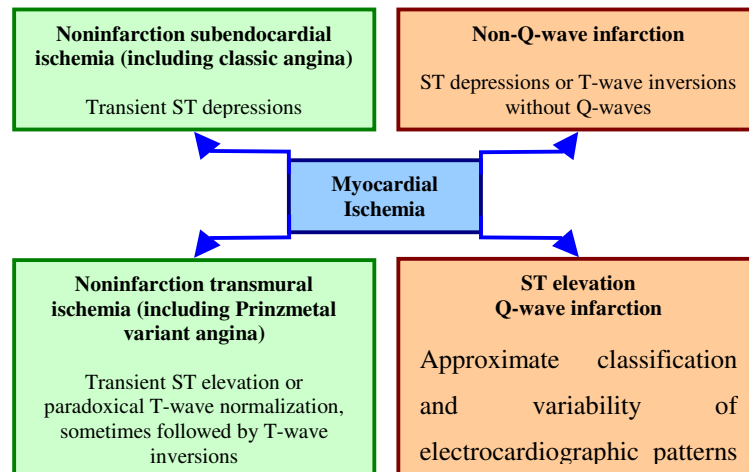

Fig. 20. A general classification, but not always accurate, of myocardial ischemia, Adopted from [13]

4.5 QRS Changes

Due to the existence of real infarctions, depolarization changes (QRS complexes) are always followed by abnormal repolarization (ST-T) [15, 24]. Necrosis of a rather large part of the myocardial tissue can lead to reductions in R-wave or Q-wave amplitude of anterior, lateral, or inferior leads. This can be a result of lack of electromotive forces in the infracted area. It was assumed in the past that abnormal Q-waves are markers of transmural myocardial infarction and subendocardial (transmural) infarctions do not make Q-waves. However, profound studies of pathological electrocardiographic signals suggested that transmural infarcts can occur with no Q-wave, or subendocardial infarcts can be accompanied by Q-waves. Therefore, a better way for the classification of infarcts is to divide them into Q-wave and Non-Q wave infarcts, instead of transmural or non-transmural infarcts [12].

4.6 Evolution of Electrocardiographic Changes

Evolution of Electrocardiographic Changes in ischemic ST-elevation and hyper-acute T-wave changes serve as the first symptoms of acute infarction. In a time period of some hours to some days, these symptoms will be followed by T-wave inversion and sometimes Q-waves. In the state of chronic ischemia or evolutionary condition, T-wave inversion will somehow be related to the long duration of the ventricular action potential and these ischemic changes are always followed by QT prolongation. After days or weeks, T-wave inversion will be resolved or will continue infinitely. The largeness of the infracted area is a good reflective of the quality of T-wave evolution (see Fig. 21). Transmural infarction with fibrosis of entire wall will exist, if T-waves have a negative value in the leads with a Q-wave. However, T-waves with a positive value in the leads with a Q-wave are a symptom of non-transmural infarction with workable myocardium of the wall [12]. The depolarization and repolarization change patterns are illustrated in Fig. 21 in the case of Q-wave infarction. Anterior-lateral infarcts will lead to ST-segment elevation in leads I, AVL, and pericardial leads which will be accompanied by ST-segment depression in the leads II, III, and AVF. On the other hand, acute inferior (or posterior) infarcts can be followed by reciprocal ST-segment depression in the leads V1 to V3. In Fig. 22, some selected samples of patterns depicted in Fig. 21 with different types of transient ST-segment episodes are simulated.

The corresponding parameter values for simulation of ST-T events during acute Q-wave infarction are presented in Table 18.
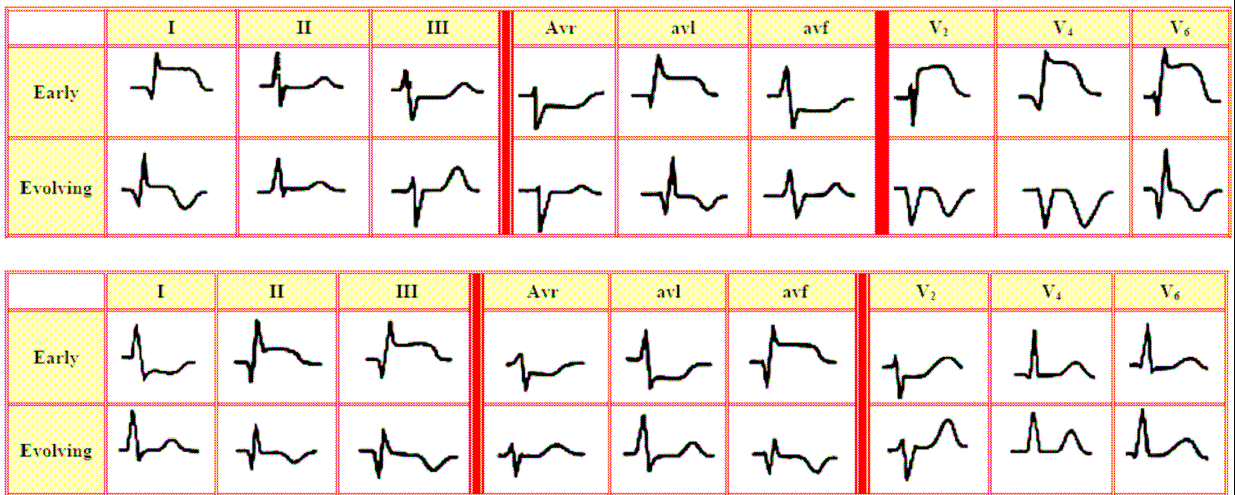
Fig. 21. Sequence of electrocardiographic patterns of depolarization and repolarization changes during Q –wave infarction in the early and evolving regimes, (top): acute anterior- lateral and (bottom): acute inferior wall Q-wave infarctions, Adopted from [12]
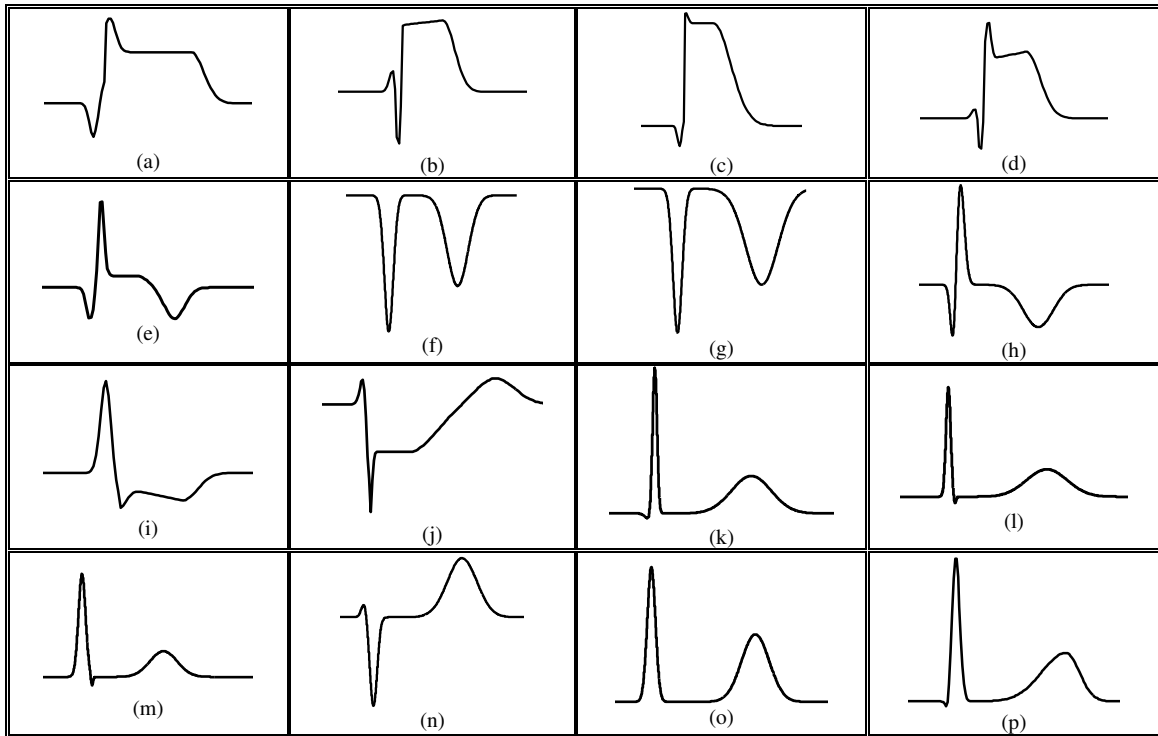

Fig. 22. Simulated ST-T episodes during acute Q-wave infarction:
Acute anterior-lateral wall Q-wave infarction in early regime for (a) lead I, (b) lead V_2, (c) lead V_4, (d) lead V_6
Acute anterior-lateral wall Q-wave infarction in evolving regime for (e) lead I, (f) lead V_2, (g) lead V_4, (h) lead V_6
Acute inferior wall Q-wave infarction in early regime for (i) lead I, (j) lead V_2, (k) lead V_4, (l) lead V_6
Acute inferior wall Q-wave infarction in evolving regime for (m) lead I, (n) lead V_2, (o) lead V_4, (p) lead V_6

Table 18. The corresponding parameters for simulation of ST-T events during acute Q-wave infarction

(a)

Parameters	Events	
	AE_1	AE_2
t_{ij}^{μ} <sec>	0.2500	0.3250
C_{ij} <mV>	-0.02	0.02
t_{ij}^{ξ} <sec>	0.0500	0.0750

$C_{ij}'(k) = 0.03 <mV>, \ m_{ij}'(k) = 0.0 <mV/sec>, \ \xi_{ij}'(k) = 0.1 <sec>$
$\xi_{ij}''(k) = 0.15 <sec>, \ \mu_{ij}'(k) = 0.3 <sec>, \ \mu_{ij}''(k) = 0.7 <sec>$

(b)

Parameters	Events	
	AE_1	AE_2
t_{ij}^{μ} <sec>	0.3000	0.3250
C_{ij} <mV>	0.01	-0.03
t_{ij}^{ξ} <sec>	0.0500	0.0250

$C_{ij}'(k) = 0.03 <mV>, \ m_{ij}'(k) = 0.01 <mV/sec>, \ \xi_{ij}'(k) = 0.1 <sec>$
$\xi_{ij}''(k) = 0.15 <sec>, \ \mu_{ij}'(k) = 0.35 <sec>, \ \mu_{ij}''(k) = 0.55 <sec>$

(c)

Parameters	Events	
	AE$_1$	AE$_2$
$\mathbf{t}_{ij}^{\mu}$ <sec>	0.3100	0.3550
C_{ij} <mV>	-0.02	0.01
$\mathbf{t}_{ij}^{\xi}$ <sec>	0.0400	0.0450

$C'_{ij}(k) = 0.1 < mV >, m'_{ij}(k) = 0.0 < mV/\sec >, \xi'_{ij}(k) = 0.0 < \sec >$
$\xi''_{ij}(k) = 0.25 < \sec >, \mu'_{ij}(k) = 0.35 < \sec >, \mu''_{ij}(k) = 0.55 < \sec >$

(d)

Parameters	Events		
	AE$_1$	AE$_2$	AE$_3$
$\mathbf{t}_{ij}^{\mu}$ <sec>	0.3000	0.3250	0.3650
C_{ij} <mV>	0.005	-0.02	0.02
$\mathbf{t}_{ij}^{\xi}$ <sec>	0.0500	0.0250	0.0350

$C'_{ij}(k) = 0.03 < mV >, m'_{ij}(k) = 0.02 < mV/\sec >, \xi'_{ij}(k) = 0.1 < \sec >$
$\xi''_{ij}(k) = 0.17 < \sec >, \mu'_{ij}(k) = 0.35 < \sec >, \mu''_{ij}(k) = 0.555 < \sec >$

(e)

Parameters	Events		
	AE$_1$	AE$_2$	AE$_3$
$\mathbf{t}_{ij}^{\mu}$ <sec>	0.2950	0.3650	0.7500
C_{ij} <mV>	-0.08	0.2	-0.08
$\mathbf{t}_{ij}^{\xi}$ <sec>	0.0550	0.0550	0.1500

$C'_{ij}(k) = 0.03 < mV >, m'_{ij}(k) = 0.0 < mV/\sec >, \xi'_{ij}(k) = 0.0 < \sec >$
$\xi''_{ij}(k) = 0.15 < \sec >, \mu'_{ij}(k) = 0.35 < \sec >, \mu''_{ij}(k) = 0.55 < \sec >$

(f)

Parameters	Events	
	AE$_1$	AE$_2$
$\mathbf{t}_{ij}^{\mu}$ <sec>	0.3350	0.8000
C_{ij} <mV>	-0.015	-0.01
$\mathbf{t}_{ij}^{\xi}$ <sec>	0.0850	0.2000

(g)

Parameters	Events	
	AE$_1$	AE$_2$
$\mathbf{t}_{ij}^{\mu}$ <sec>	0.3350	0.9000
C_{ij} <mV>	-0.015	-0.01
$\mathbf{t}_{ij}^{\xi}$ <sec>	0.0850	0.3000

(h)

Parameters	Events		
	AE$_1$	AE$_2$	AE$_3$
$\mathbf{t}_{ij}^{\mu}$ <sec>	0.2900	0.3350	0.9000
C_{ij} <mV>	-0.015	0.02	-0.008
$\mathbf{t}_{ij}^{\xi}$ <sec>	0.0600	0.0850	0.3000

(i)

Parameters	Events	
	AE$_1$	AE$_2$
$\mathbf{t}_{ij}^{\mu}$ <sec>	0.2900	0.3350
C_{ij} <mV>	0.2	-0.05
$\mathbf{t}_{ij}^{\xi}$ <sec>	0.0600	0.0850

$C'_{ij}(k) = 0.03 < mV >, m'_{ij}(k) = 0.1 < mV/\sec >, \xi'_{ij}(k) = 0.0 < \sec >$
$\xi''_{ij}(k) = 0.15 < \sec >, \mu'_{ij}(k) = 0.35 < \sec >, \mu''_{ij}(k) = 0.6 < \sec >$

(j)

Parameters	Events		
	AE$_1$	AE$_2$	AE$_3$
$\mathbf{t}_{ij}^{\mu}$ <sec>	0.2950	0.3400	1.1500
C_{ij} <mV>	0.02	-0.06	0.03
$\mathbf{t}_{ij}^{\xi}$ <sec>	0.0450	0.0400	0.4500

$C'_{ij}(k) = 0.05 < mV >, m'_{ij}(k) = 0.0 < mV/\sec >, \xi'_{ij}(k) = 0.0 < \sec >$
$\xi''_{ij}(k) = 0.35 < \sec >, \mu'_{ij}(k) = 0.35 < \sec >, \mu''_{ij}(k) = 0.6 < \sec >$

(k)

Parameters	Events		
	AE$_1$	AE$_2$	AE$_3$
$\mathbf{t}_{ij}^{\mu}$ <sec>	0.3150	0.3400	0.9500
C_{ij} <mV>	-0.01	0.2	0.05
$\mathbf{t}_{ij}^{\xi}$ <sec>	0.0750	0.0400	0.3500

(l)

Parameters	Events		
	AE$_1$	AE$_2$	AE$_3$
$\mathbf{t}_{ij}^{\mu}$ <sec>	0.2900	0.3800	0.9500
C_{ij} <mV>	0.2	-0.015	0.05
$\mathbf{t}_{ij}^{\xi}$ <sec>	0.0900	0.0200	0.3500

(m)

Parameters	Events		
	AE$_1$	AE$_2$	AE$_3$
$\mathbf{t}_{ij}^{\mu}$ <sec>	0.3800	0.3150	0.8500
C_{ij} <mV>	-0.02	0.2	0.05
$\mathbf{t}_{ij}^{\xi}$ <sec>	0.0200	0.0650	0.2500

(n)

Parameters	Events		
	AE$_1$	AE$_2$	AE$_3$
$\mathbf{t}_{ij}^{\mu}$ <sec>	0.2900	0.3550	1.5000
C_{ij} <mV>	0.021	-0.12	0.08
$\mathbf{t}_{ij}^{\xi}$ <sec>	0.0600	0.0750	0.2000

<table>
<tr><td rowspan="2">(o)</td></tr>
</table>

Parameters	Events	
	AE$_1$	AE$_2$
$\mathbf{t}_{ij}^{\mu}$ <sec>	0.2750	1.000
C_{ij} <mV>	0.2	0.1
$\mathbf{t}_{ij}^{\xi}$ <sec>	0.0750	0.2000

(o)

Parameters	Events	
	AE$_1$	AE$_2$
$\mathbf{t}_{ij}^{\mu}$ <sec>	0.3050	0.3550
C_{ij} <mV>	-0.02	0.15
$\mathbf{t}_{ij}^{\xi}$ <sec>	0.0450	0.0750

(p)

$$C'_{ij}(k) = 0.05 < mV >, \ m'_{ij}(k) = 0.0 < mV / \sec >, \ \xi'_{ij}(k) = 0.3 < \sec >$$
$$\xi''_{ij}(k) = 0.2 < \sec >, \ \mu'_{ij}(k) = 1.1 < \sec >, \ \mu''_{ij}(k) = 1.1 < \sec >$$

4. 7 Discussion

In the previous sections, generation of different arrhythmias using the presented model was demonstrated. Because of the fact that arrhythmias are the result of abnormal occurrences with occasionally distinct natures in the heart electrical activity [12], the modification of FEM-based or electrical element-based models to generate any kind of abnormal ECG signal can be difficult or even impossible. The major advantage of the presented model is its high capability in the generation of approximately all observed arrhythmias including transient or permanent phenomena. Therefore, this model will enable the user to generate the desired signal in any shape by first choosing a suitable structure of the model and then its parameterization. In Fig. 23, a procedure for the model application in arrhythmias classification is illustrated. In this method, the ECG signal is preprocessed and the corresponding base-line wander is removed. Then, a specific segment such as ST-segment, RR interval, PR interval, etc is picked up from the ECG signal. Finally, the same segment is parameterized by the presented model for a certain arrhythmia and the model parameters are approximately estimated using a nonlinear adaptive algorithm like nonlinear least squares (Gauss-Newton Approximation) or maximum likelihood (Newton-Raphson Approximation) [22]. Provided a high accordance between the estimated output of the nonlinear adaptive filter and the actual ECG signal, it can be concluded that the certain arrhythmia will exist in the ECG signal with a high incorporation.

The alternate usage of the developed model is that the model parameters of each arrhythmia can be assigned to its specific class and therefore, different sets of parameter values for different arrhythmias can be obtained. If the intersection of the resulted parameter sets is not high, the status of the real present signal can be assigned to its proper class by implementing an appropriate classification algorithm. Consequently, the arrhythmia(s) are detected.

In Fig. 24, another scheme of the application of the presented model is developed. In this plan, a specific segment of the actual ECG signal is selected and the corresponding segment is simulated by the model. Then, a suitable transform (such as wavelet or any other kind of time-frequency transforms) is taken from both the real and simulated signals. Finally, the obtained parameters are compared together using a specific classification algorithm such as principal component analysis (PCA) or independent component analysis (ICA) and the fitness percentage of the actual signal to the certain arrhythmia is approximately calculated.

In summary, it can be stated that in the first plan the structure of the model is implemented for the parameter classification, however, in the second approach, the model output is used as a classification tool. Both these tests are currently under study and the results will be presented in the future work.
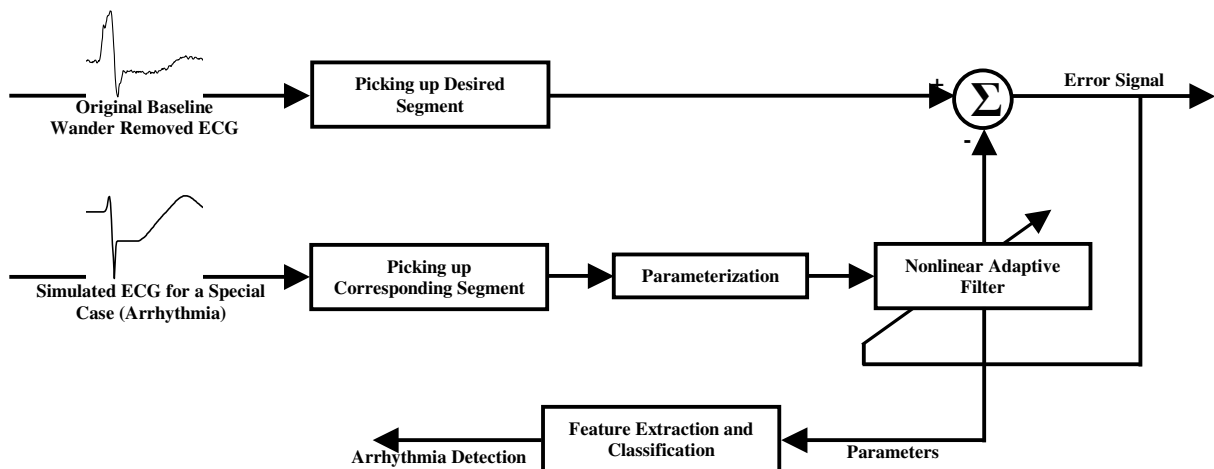

Fig. 23. An adaptive scheme for use of the proposed model. In this methodology a nonlinear adaptive filter is used to identify the parameters of the artificial model. Obtained parameters, filter output or both can be used for the purpose of classification.
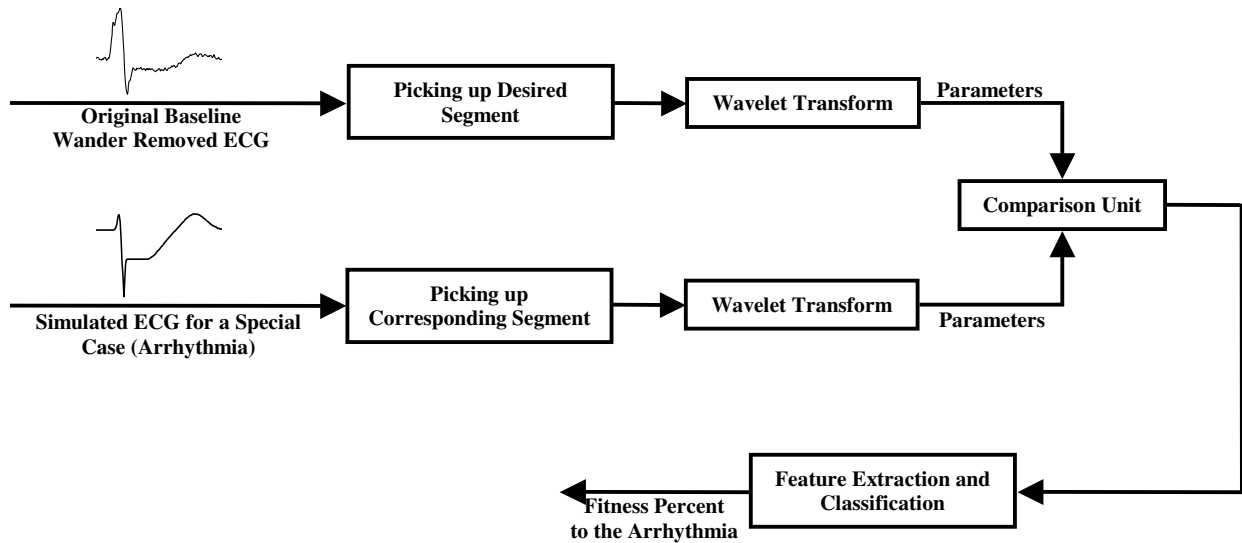
Fig. 24. A secondary scheme for identification of arrhythmia based on an appropriate time-frequency transformation. In this method a time-frequency transformation is taken from the original signal and the simulated corresponding signal and feature spaces are constructed. Then a suitable classifier is used to find the dominant abnormal phenomenon.

5 Conclusion

In this study, we developed a mathematical model based on algebraic equations to generate artificially normal events of electrocardiogram (ECG) signals such as P-wave, QRS complex, and T-wave. This model was also implemented for the simulation of abnormal phenomena of electrocardiographic signals such as ST-segment episodes (i.e. depression, elevation, and sloped ascending or descending) and repolarization abnormalities such as T-Wave Alternans (TWA). The presented model was also used for the simulation of ECG signals on torso plane or limb leads. To meet this end, the amplitude of events in each of the 15-lead ECG waveforms of 80 normal subjects at MIT-BIH Database (**www.physionet.org**) are derived using wave- detector module existing in Waveform Database (WFDB) and then recorded. Various statistical

analyses such as amplitude mean value, variance and confidence intervals calculations, Anderson-Darling normality test, and Bayesian estimation of events amplitude were next conducted. Heart Rate Variability (HRV) model was also incorporated to this model with HF/LF and VLF/LF waves power ratios. Eventually, in order to demonstrate good flexibility of the presented model in simulation of ECG signals, left septal ventricular tachycardia, rate dependent conduction block (Aberration), and acute Q-wave infarctions of inferior and anterior-lateral walls were finally simulated. The source code (Matlab® m-file) of the proposed computer model is distributed freely in the hope that it will be useful for cardiologists and biomedical engineers.

References

[1] Sachse F. B., *"Computational Cardiology, Modeling of Anatomy, Electrophysiology, and Mechanics"*, Springer-Verlag Pub., Berlin Heidelberg 2004.

[2] Söderström T., Stoica P, "System Identification",Hemel Hempstead, *UK:* Prentice-Hall International, 1989.

[3] Killmann R., Wach P. and. Dienstl F, "Three-dimensional computer model of the entire human heart for simulation of reentry and tachycardia: Gap phenomenon and Wolff-Parksinson-White syndrome", *Basic Research in Cardiology*, Vol. 86, No. 5, pp. 485–501, 1991.

[4] Rogers J. M., "Modeling the cardiac action potential using b-spline surfaces", *IEEE Transactions on Biomedical Engineering*, vol. 47, no. 6, pp. 784–791, June 2000.

[5] McSharry P. E., Clifford G. D., Tarassenko L., and Smith L. A., "A Dynamical Model for Generating Synthetic Electrocardiogram Signals", *IEEE Transactions on Biomedical Engineering*, Vol. 50, No. 3, March 2003.

[6] Kandori, Shimizu W., Yokokawa M., Kamakura S., Miyatake K., Murakami M., Miyashita T., Ogata K., Tsukada K., "Reconstruction of Action Potential of Repolarization in Patients with Congenital Long QT Syndrome", *Physics in*

Medicine and Biology, Vol. 49, pp. 2103-2115, 2004.

[7] Clifford G. D., Sameni R., "An Artificial Multi-Channel Model for Generating Abnormal Electrocardiographic Rhythms", *Proceeding of the Computers in Cardiology (CinC) Conference*, 2008.

[8] Serinagaoglu Y., MacLeod R. S., Yilmaz B., Brooks D.H., "Epicardial mapping from venous catheter measurements, body surface potential maps, and an electrocardiographic inverse solution", *J. Electrocardiol.*,Vol. 35,pp.65–74, 2002.

[9] Groenewegen A. S., Lesh M. D., Roithinger F. X., Ellis W. S., Steiner P. R., Saxon L. A., Lee R. J., Scheinman M. M., "Body Surface Mapping of Counterclockwise and Clockwise Typical Atrial Flutter: A Comparative Analysis With Endocardial Activation Sequence Mapping", *Journal of the American College of Cardiology* ,Vol. 35, No. 5, 2000.

[10] Hampton J. R., *"The ECG Made Easy"*, Churchill Livingstone Pub., Six Edition, 2002.

[11] Ashley E. A., Niebauer J.,*"Cardiology Explained*", Remedica Pub., 2005.

[12] Libby P., Bonow R.O., Mann D. L., Zipes D. P., "*Braunwald's Heart Disease: A Textbook of Cardiovascular Medicine*", Saunders, 8th edition, , 2007.

[13] Montgomery D. C., Runger G. C., *"Applied Statistics and Probability for Engineers* ", John Wiley & Sons ,Third Edition, 2003.

[14] Task Force of the European Society of Cardiology, the North American Society of Pacing, and Electrophysiology, "Heart Rate Variability: Standards of Measurement, Physiological Interpretation, and Clinical Use," *Sophia Antipolis*, Vol. 93 ,1996

[15] Jager F., Moody G. B., Mark R. G., "Detection of Transient ST-Segment Episodes During Ambulatory ECG Monitoring", *Computers and Biomedical Research*, Vol. 31, pp. 305-322, 1998.

[16] Moody G. B., "*WFDB Applications Guide"*, Harvard-MIT Division of Health Sciences and Technology, Tenth Edition, 2006. (http://www.physionet.org/physiotools/wag/)

[17] Gray R. M. and Davisson L. D., *"An Introduction to Statistical Signal Processing"*, Cambridge University Press , 2007

[18] J. G. Webster, "Medical Instrumentation: Application and Design", *John Wiley & Sons*, Third Edition, 1998

[19] Malmivuo J., Plonsey R., *"Bioelectromagnetism Principles and Applications of Bioelectric and Biomagnetic Fields"*, Oxford University Press, 1995

[20] Van Capelle F. J. and Durrer D., " Computer simulation of arrhythmias in a network of coupled excitable elements ", *Circulation Research*, Vol. 47, No. 3, pp. 454-466, 1980

[21] Ghaffari, M. R. Homaeinezhad, M. Atarod, R. Rahmani, "Detecting and Quantifying T-Wave Alternans Using the Correlation Method and Comparison with the FFT Based Method", *Proceeding of the Computers in Cardiology (CinC) Conference*, 2008

[22] Anderson B.D. O.,Moore J.B., *"Optimal Filtering"*, Prentice- Hall Inc. 1979

[23] Hsu H. P., *"Theory and Problems of Probability, Random Variables, and Random Processes"*, McGraw-Hill, 1997

[24] Ghasemi M., Jalali A., SadAbadi H., Ghorbanian P., Atarod M., Golbayani H., Ghaffari A. "Electrocrdiographic Imaging of Myocardial Infarction Using Heart Vector Analysis",*Computers in Cardiology*, Vol. 37, pp. 625-628, 2007.

Ali Ghaffari, Professor of Mechanical Engineering at K. Nassir Toosi univ. of Technology, Tehran, Iran.
(Ph.D.): University of California at Berkeley, Dept. of Mechanical Eng., California, USA.
(M.Sc.): Georgia Institute of Technology, Dept. of Mechanical Eng., USA.
(B.Sc.): Sharif University of Technology Dept. of Mechanical Eng., Tehran, Iran.
His research interests include nonlinear dynamics and control, analysis of stochastic phenomena, Fuzzy systems, Artificial Neural Networks, ANFIS, and biomedical signal processing and control.
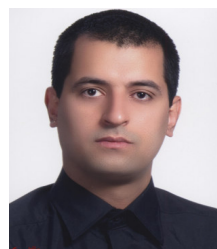
Mohammad Reza Homaeinezhad was born in Shiraz, Iran, in 1980. He received the B.S. and the M.S. degrees (with the best honors) both in Mechanical engineering- Dynamic systems and control- from K. Nassir Toosi univ. of Technology, Tehran, Iran in 2003 and 2005 respectively. He is currently Ph.D. candidate of Mechanical engineering in K. Nassir Toosi univ. of Technology. His research interests include nonlinear dynamics and control, statistical signal analysis and parameter estimation, automatic decision making (detection & modulation) theory and biomedical waveforms (BP, ECG & PCG) processing.

Yashar Ahmadi was born in Munchen, Germany in 1982. He received the B.S. degree (with the best honor) in Mechanical engineering- Vibration- from Shahrood univ. of Technology, Semnan, Iran in 2006. Now, he is pursuing toward his Ms.c. degree at K. Nassir Toosi univ. of Technology.

Mostafa Rahnavard was born in Sabzevar, Iran in 1986. He received the B.S. degree (with the best honor) in Mechanical engineering- Dynamic systems and control- from K. Nassir Toosi univ. of Technology, Tehran, Iran in 2008. Now, he is pursuing toward his Ms.c. degree at Sharif University of Technology.

Reza Rahmani Assistant professor of Cardiology at Tehran University of Medical Science, and a member of Cardiovascular and Catheter unit of Imam Khomeini hospital, Tehran, Iran.